Università Politecnica delle Marche

PhD School in Human Health Research

Neuronal nitric oxide synthase positive cells in the human corpus callosum and indusium griseum

Ph.D. Dissertation of:

Dr. Andrea Sagrati

Tutor:

Prof. Mara Fabri

Second Tutor:

Dr. Teresa Lorenzi

Curriculum supervisor:

Prof. Mario Guerrieri

Università Politecnica delle Marche

Department of Experimental and Clinical Medicine

Via Tronto 10A - 60126 - Torrette di Ancona, Italy

CONTENTS

1. ABSTRACT

The aim of the present study is to investigate the possible mechanism for the control of cerebral blood flow in the human corpus callosum (CC), that could explain the BOLD (blood-oxygen-level dependent) effect previously found (Fabri et al., 2011). This effect is a signal of reactive hyperemia which has long been believed to be associated to grey matter. The observation that the BOLD effect can also be evoked in the white matter of the corpus callosum is a very recent finding that is attracting a great interest from a growing number of researchers.

To this purpose, the cellular component of CC was analyzed. Particular attention was payed to study the presence, distribution, morphology and number of neuronal Nitric Oxyde Sinthase (nNOS) positive cells in this anatomical structure and in the overlying indusium griseum (IG).

Nitric Oxyde (NO) is a gaseous neurotransmitter largely diffused in the brain, which exerts a powerful vasodilatory effect, and can therefore contribute to regulate the cerebral blood flow.

Sagittal serial sections from paraffin or frozen autoptic specimens of human adult CC and overlying IG were processed for immunohistochemistry and immunofluorescence analysis, using an antibody against nNOS whose quality was tested by Western Blot. The stainings revealed the presence of many nNOS immunopositive cells. By double labeling technique with immunofluorescence at confocal microscopy, neurons positive to nNOS antibody were observed in CC and IG. Neurons showed different morphologies, were more numerous 1 mm apart from the medial line in IG and 4 mm in CC, with a peak over the body of the CC. In some cases, they were located at the boundary between IG and CC, more densely packed in proximity to the pial arteries penetrating into the CC. The significant presence of nNOS immunopositive neurons in these two structures suggests that they might have a role in the neurovascular regulation of CC and that IG is not a merely rudimentary tissue but likely plays a functional role in the adult brain.

The presence of nNOS positive astrocytes in the human CC has been here demostrated for the first time. Their number and distribution varied in different conditions: nNOS positive astrocytes were

absent in samples from subjects deceased after a short hypoxia; their number and labeling intensity increased with the hypoxia prolongation. Neuronal NOS immunopositivity of CC astrocytes seems thus related to the hypoxia duration and the consequent brain damage and therefore it is suggestive of a potential role of astrocytes in the control of cerebral blood flow.

2. INTRODUCTION

2.1 Corpus callosum

To perform complex tasks, mammals require coordinated brain activity, based on precise and efficient connections between the two hemispheres. These connections consist of axons that traverse the telencephalic midline, principally in three commissural tracts: the corpus callosum, the hippocampal commissure and the anterior commissure. Among these, the corpus callosum (CC) is the most voluminous fiber tract, and in the human species it reaches its maximum complexity and size respect to all the other placental mammals (Gazzaniga, 2000).

The corpus callosum (CC) is the largest neural pathway interconnecting the two cerebral hemispheres (Innocenti, 1986). It is located in the bottom of the fissura longitudinalis cerebri, inferior to cortex and superior to the thalamus. It is approximately 10 cm in length and is C-shaped in a gentle upwardly convex arch (Gray et al., 2017). The CC can be divided into five anatomical regions; from rostral to caudal direction, they are the genu, the rostrum, the body or trunk (often subdivided into anterior, middle and posterior body), the isthmus, and the splenium (Fabri et al., 2014). There are no clear borders between regions, but the different callosal regions have different fiber compositions: large diameter fibers have been described in the posterior part of the splenium and in the body (Aboitiz et al., 2003; Aboitiz et al., 1992), where interhemispheric sensory fibers cross the commissure and exchange information at high speed; small fibers mainly connecting association cortical areas are found in the rostrum, genu and anterior body (Aboitiz et al., 1992, 2003). Immediately above the body of the CC, lies the interhemispheric fissure in which the falx cerebri runs together with branches of the anterior cerebral vessels. The superior surface of the corpus callosum is covered by a thin layer of grey matter known as the indusium griseum (IG). On either side, the body is separated from the cingulate gyrus by the callosal sulcus. Attached to the concave undersurface of the corpus callosum is the thin vertical septum pellucidum anteriorly, and the fornix and its commissure posteriorly (Gray et al., 2008).

The CC is a recent phylogenetic acquisition of placental mammals, developing by fusion of the interhemispheric midline fibers with specialized midline glial cells guiding callosal fibers to the contralateral side (Raybaud, 2010). It originates from the glial sling, above and rostral to the anterior and hippocampal commissures: it thus forms from the fusion of two separate segments. The development of the CC is a dynamic and complex event where callosal axons first surround the ipsilateral ventricular system and then turn medially across the midline and grow into the opposite hemisphere towards the homotypical target area, interacting with different cellular structures and the extracellular matrix (Rakic and Yakovlev, 1968; Richards et al., 2004). The midline zipper glia, glial wedge and the indusium griseum (IG) glia are transient cellular structures situated along the midline that have been shown to play critical roles in the guidance of the pioneering axons of the corpus callosum during the development (Silver et al., 1993; Shu et al., 2003).

The anterior, sling-derived callosum (containing fibers connecting frontal associative and possibly primary sensory-motor areas of the two hemispheres) and the hippocampal commissure-associated splenium (containing fibers arising in the parietotemporo-occipital cortex and directed to the opposite hemisphere) probably fuse just anterior to the hippocampal commissure (Raybaud, 2010). The CC grows in size by the increase of the connectivity and the tangential growth of the cortex. In the womb and in the early postnatal period it mainly grows by fiber addition, whereas later increases are due to the development of myelin, which offsets pruning of callosal fibers; fiber myelination becomes significant at about 6 months of postnatal life in the splenium and at about 8 months in the genu. Myelination is believed to proceed from posterior to anterior (Deoni et al., 2011; Provenzale et al., 2012), reflecting the fact that myelination of primary cortical areas (somatic sensory, motor, auditory, visual) connected through the isthmus and splenium predates the myelination of the body, genu, and rostrum, which are related to the more anterior associative areas.

The CC comprises myelinated (70%) and unmyelinated (30%) axons and glial cells (glia) (Innocenti, 1986). Callosal axons originate from neurons located in layers II/III and V of the cerebral cortex (Innocenti, 1986). The great majority of such axons use glutamate (Glu) as neurotransmitter

(Barbaresi et al., 1987), whereas a very small percentage use γ-aminobutyric acid (GABA) (Fabri and Manzoni, 2004; Higo et al., 2009). Glutamate is the most abundant neurotransmitter in the vertebrate nervous system and it is involved in most excitatory function in the vertebrate brain (Meldrum, 2000). Glu is released in the CC by unmyelinated fibers at specific axon–glia synaptic junctions (Ziskin et al., 2007). GABA is the chief inhibitory neurotransmitter in the mammalian central nervous system (Watanabe et al., 2002). However, the mechanism through which an inhibitory effect may be eventually be exerted by callosally-projectung GABAergic neurons has not yet been clarified. In the mature CC, glial cells include oligodendrocytes (ODCs) and astrocytes. ODCs produce myelin, a fatty white substance surrounding the axon that originates an electrically insulating layer whose main purpose is to increase the speed at which impulses propagate along the myelinated fiber. Astrocytes are thought to play a number of active roles in the brain, including the secretion or absorption of neural transmitters and maintenance of the blood–brain barrier. Aside from glial cells, the CC also contains neurons, as demonstrated by immunocytochemical studies in the CC of cat (Riederer et al., 2004), rat (Revishchin et al., 2010; Barbaresi et al., 2014; Barbaresi et al., 2018), and monkey (Rockland et al., 2012). Intracallosal neurons have been described also in human brain in a very recent paper (Milosˇevic et al., 2010), in which the morphology, molecular phenotypes and distribution of neurons were studied.

The CC has a rich blood supply by arteries that originate from the pericallosal artery, the portion of the anterior cerebral artery (ACA) located distal to the anterior communicating artery (ACoA) (Kahilogullari, 2008). The branches that depart from ACoA have been classified differently by various authors. There is no classic and/or standard definition for the callosal branches of the pericallosal artery. We based our classification on that used by Ture et al. (1996), where the main branches, classified on diameter and average number for hemisphere, are: short callosal arteries, cingulocallosal arteries, recurrent cingulocallosal arteries, long callosal arteries and median callosal arteries. These branches supply blood to the body and genu of corpus callosum and they are called pericallosal pial plexus (Malobabic', 1982); a different refueling of blood is found in splenium. In

particular, vascular supply to the splenium was provided by the anterior pericallosal artery (40% of observed cases) from the anterior circulation and by the posterior pericallosal artery (88%) and posterior accessory pericallosal artery (50%) from the posterior circulation (Kahilogullari et al., 2012).

Over the last few years a rising number of functional magnetic resonance imaging (fMRI) studies reported an activation of white matter, particularly the CC. Functional MRI allows to study the intact brain non invasively. It is a functional neuroimaging approach based on MRI technology that measures brain activity by detecting associated changes in blood flow, based on the well-established notion that neuronal activation in an area of the brain is accompanied by a local increase in blood flow. The blood-oxygen-level dependent (BOLD) effect is a method based on the different ratio of oxygenated to deoxygenated hemoglobin in blood. Given that the two forms of the molecule have different magnetic behaviors, the change of their relative concentration, due to an increase in blood flow evoked by increased neural activity, generates a magnetic-electric signal that is detected by the equipment, highlighting the areas of the brain that are active at any given time. The BOLD signal thus reflects the haemodynamic responses coupled to neuronal signaling processes (Iadecola, 2004; Lauritzen, 2005). It has long been believed that the BOLD effect is mainly due to the metabolic activity associated with synaptic rather than spiking activity, and therefore it could be evoked only in gray matter (Logothetis et al., 2001). However, data from the newer imaging techniques suggest that a hemodynamic response can also be evoked in white matter, particularly in the CC. These findings were at first observations sporadically recorded during interhemispheric transfer tasks performed by subjects within the magnet (Tettamanti et al., 2002; Mazerolle et al., 2008), or during activities not involving specific interhemispheric transfer tasks, such as voluntary swallowing (see Fabri et al., 2014, for a review). Recent studies examined the BOLD effect evoked in the CC by simple sensory stimuli or by the performance of motor tasks activating the cortical areas which in healthy control subjects harbor the representation of motor activation and of gustatory, olfactory, auditory, visual and tactile sensitivity (Fabri et al., 2011, 2013; Polonara et al., 2014). These studies did detect consistent

activation foci in discrete regions of the CC: anterior (olfactory and gustatory stimulation), central (motor tasks), central-posterior (touch stimulation), isthmus (auditory stimulation) and splenium (visual stimulation), thus confirming the existence of a topographic organization of the CC from a functional point of view, demonstrating that it may be investigated using fMRI. The presence of a BOLD signal in the white matter has been explained with the involvement of astrocytes, which would act on vessel dilation to meet the greater metabolic and oxygen demand due to the activity induced by stimulation (Gawryluk et al., 2014; Petzold et al., 2011). The astrocytes are thus one of the possible actors regulating cerebral bood flow (CBF) during changes of oxygen supply or demand, as it can occur during physiological (increased activity) or even pathological (hischemia) conditions. The action of astrocytes can be exerted by modulating the synthesis and/or release of nitric oxide (NO), a vasoactive agent largely diffused in the brain, which participates in numerous physiological functions, including that of a neurotransmitter. A recent study (Simic et al., 2000) provided the first evidence that production of NO in Alzheimer's Disease in human hippocampus and entorhinal cortex is upregulated by nNOS activation in reactive astrocytes. In addition, another study demonstrated the rapid and massive iNOS-dependent NO production by astrocytes in situ, which appeared to be triggered by acute neuronal death in mouse neocortex (Buskila et al., 2005). Nitric oxide is synthesized by NO synthase (NOS) from L-arginine and, being a gaseous molecule, simply diffuses from nerve terminals, as opposed to the exocytosis by which conventional neurotransmitters are released. Nitric oxide ca be produced at least by three isoforms of NOS: neuronal (nNOS), endothelial (eNOS) and inducible (iNOS) (Dawson et al., 1994; Zhang et al., 1995). The physiological sphere of influence of NO has been estimated at about 200 – 400 μm, corresponding to a volume of brain enclosing 2 million synapses (Estrada et al., 1998; Wood et al., 1994; Laranjinha et al., 2012). It is known that NO regulates the response to hypoxia, especially when oxygen delivery is reduced in the absence of hypoxemia (low oxygen saturation or partial pressure of oxygen; Ho et al., 2012). Neurons immunopositive to nNOS that could induce an haemodynamic response have been recently described in the rat CC (Barbaresi et al., 2014).

2.2 Indusium griseum

The human indusium griseum (IG), or gyrus epicallosus, or gyrus supracallosus, consists of a symmetric pair of thin cortices that are a ventromedial continuation of the cingulate gyrus on each side of the midline, and covering the dorsal surface of the CC. Myelinated fibers cover the IG along the medial and lateral portions of the midline, namely the medial and lateral longitudinal striae of Lancisi (Di Ieva et al., 2007, Di Ieva et al., 2015). The development of the IG and its neuronal and glial differentiation have been quantitatively studied in the mouse brain (Sturrock 1977, 1978a, 1978b, 1978c). According to these studies, the IG is generally considered a rudiment of the dorsal extension of the hippocampal formation (supracommissural hippocampus), similar to the dentate gyrus (DG) (Rasonja et al., 2019). Therefore, it could be considered a component of the limbic system (Di Ieva et al., 2015), but it is still unclear whether IG is an embryological remnant or an active functional component of it. A very recent paper carried out in humans (Rasonja et al., 2019) found that IG is developmentally distinct from the hippocampal formation; in addition, it exhibits continued maturation, even in the final trimester of gestation, with no signs of regression during the fetal period, suggesting that it is not merely a rudimentary tissue, but plays a role in the adult brain as well (Rasonja et al., 2019). Moreover, a Golgi (Wyss et al., 1983) and an immunocytochemical study (Barbaresi et al., 2018) in rat described the presence of neurons within the IG, corroborating the hypothesis that IG has an its functional autonomy. For the IG, as for the CC, the primary blood supply is provided by the callosal arteries which originate from the pericallosal artery (Kakou et al., 2000; Ugur et al., 2006). The callosal arteries give rise to branches that perfore the IG and then get deep in CC.

3. AIM OF THE STUDY

The human brain has a high-energy demand, and the cerebral blood flow (CBF) is critically important for brain function and viability, delivering nutrients and oxygen (Fantini et al., 2016). When the activity of a brain region increases, CBF to that region also increases. This mechanism, termed functional hyperaemia, controls not only the substrate and oxygen delivery, but also the removal of by-products of metabolism. (Iadecola, 2004). Many neurotransmitters play a key role in the regulation of CBF by modulating vascular tone, one of which is the NO.

The aim of the present study is to elucidate the morphological basis of the control of CBF in the CC, with the intent to explain the BOLD effect previously found (Fabri et al., 2011, 2013, 2014). To this purpose, the presence, distribution and morphology of NO producing cells in the human adult CC and IG was investigated.

4. MATERIALS AND METHODS

4.1 Tissue sources and preparation

Human autoptic brains were obtained from 20 adutlt subjects without known neurological pathologies. The gender, age at death, and postmortem-interval (PMI) (i.e. the time between death and the autopsy) were registered, and reported in Table 1.

In order to remove the CC and the overlying IG, the interhemispheric fissure of each brain was exposed and gently retracted. The resulting tissue samples were prepared for biochemical (Western Blot, WB) and/or morphological (histochemistry, immunohistochemistry and immunofluorescence) analysis. Only samples with no macroscopically or microscopically signs of neuropathological alterations and decomposition were included in the analysis. Samples for WB analyses were immediately frozen in liquid nitrogen and stored at –80°C; samples for morphological analyses were fixed for 11 days in 4% neutral buffered formalin at 4°C, then embedded in paraffin, to obtain thin sections for qualitative analysis, or frozen to perform quantitative analysis.

All procedures performed for the sampling of autoptic tissue were approved by the Ethics Committee of Università Politecnica delle Marche and conducted in accordance with the Helsinki Declaration of 1975, as revised in 2013. Need for consent was waived by the Ethics Committee. In addition, the samples were made anonimous and linked exclusively to codes.

4.2 Western Blot

Western blot analysis was performed in order to to test the quality of anti-human nNOS primary antibody used in immunohistochemistry. To this purpose, only IG was processed.

Indusium griseum specimens from two cases (10 and 11) were obtained by mechanical detachment of IG from the CC, immediately after the removal of the biopsy from the brain. Tissue lysates of IG specimens were prepared after complete Potter homogenization on ice (Ultra-Turrax T8, IKA-WERKE, Lille, F) in lysis buffer containing 1% Triton X-100, 50 mM HEPES, pH 7.5, 150 mM

NaCl, 10% glycerol, 1.5 mM $MgCl_2$, 5 mM EGTA and protease inhibitors (Pefabloc SC; Complete Roche Diagnostic S.p.A.) freshly added. As a control of the method used, rat CC tissue lysate known to contain nNOS protein (Barbaresi et al. 2014) was analyzed in WB. Protein concentrations were assessed with Bradford protein assay (Bio-Rad Laboratories, Milano, Italy). Equal amounts of proteins (500 µg) were denatured with sample buffer, boiled for 5 min, and fractionated on 8% SDS-polyacrilamide gels (SDS-PAGE). Blots were first incubated with 5% BSA (Bovine Serum Albumin; Sigma, Milano, Italy) in TBS-T 0.5% and then overnight at 4 C° with anti-human nNOS policlonal antibody made in rabbit (Cayman Chemical, Hambrug, Germany) (Table 2) diluted 1:700 in TBS. After washing, blots were incubated with anti-rabbit secondary antibody conjugated to horseradish peroxidase (Amersham Italia srl, Milano, Italy) (Table 3) diluted 1:5000 in TBS. Detection of bound antibody was performed with ECL-Western blotting detection kit (Amersham) according to the manufacturer's instructions.

4.3 Immunohistochemistry

To detect and characterize the nNOS immunopositive cells in the CC and IG, immunohistochemistry (IHC) technique on paraffin sections was used. The quantitative analysis was performed by immunohistochemistry on frozen sections because this method allows to obtain thicker sections and thus to cut CC and overlying IG in their entire thickness.

The samples from each case weres fixed for 11 days in 4% phosphate-buffered paraformaldehyde (0.1 M phosphate buffer, pH 7.4) at 4C°, and processed a to obtain paraffin and/or frozen sections.

4.3.1 Paraffin sections

Small tissue blocks of callosal genu from all cases were embedded in paraffin and cut in 15-µm-thick sagittal serial sections. Paraffin sections were deparaffinized and rehydrated via xylene and a graded series of ethyl alcohol.

To delineate the boundaries and cellular compartments of the midline structures, sections were stained by Luxol fast blu (Bio-Optica, Milano, Italy) and eosin (Bio-Optica) allowing to identificate the IG.To inhibit endogenous peroxidase activity, sections were incubated for 30 min with 3% hydrogen peroxide in methanol. Sections were then washed in phosphate-buffered saline (PBS). For the detection of Neuronal marker Nuclei (NeuN) (a neuronal marker) and Glial Fibrillary Acidic Protein (GFAP) (a marker for astrocytes), sections were retreated in a water bath for 30 minutes at 90 C° in 0.1 M sodium citrate (pH 7.2), according to antibody datasheet. The sections were incubated with BSA (Sigma) for 1 h at room temperature (RT) to block nonspecific background.

Sections were then incubated overnight at 4 C° with one of the following primary antibodies (Table 2): a) anti-human nNOS policlonal antibody made in rabbit (Cayman Chemical) diluted 1:500 in PBS; b) anti-human NeuN monoclonal antibody made in mouse (Merck, S.p.a., Milano, Italy) diluted 1:100 in PBS; c) anti-human Alpha-Smooth Muscle Actin (α-SMA) (a marker for mature myofibroblasts) monoclonal antibody made in mouse (Agilent Dako, Santa Clara, CA, USA) diluted 1:100 in PBS; d) anti-human GFAP made in rabbit (Merck, Milano, Italy) diluited 1/100 in PBS.

After washing in PBS, the sections were incubated for 1 h at RT with biotinylated goat anti-rabbit (bGAR) or goat anti-mouse (bGAM) secondary antibody (Vector Laboratories, Burlingame, CA) (Table 3) diluted 1:200 in PBS. The Avidin-Biotin-Complex with peroxidase method (ABC; Vector Laboratories) was performed for 1 h at RT, and 3-3’ diaminobenzidine hydrochloride (DAB; Sigma-Aldrich, St Louis, MO, USA) was used as chromogen. Normal human renal tissue was used as positive control for nNOS because macula densa cells produce this protein (Lorenzi et al., 2020). Negative controls were performed by omitting the primary or the secondary antibodies. The negative controls confirmed the specificity of the immunolabeling obtained with the primary antibodies. Immunostained sections are observed in light microscopy under a motorized Leica DM6000 microscope at different magnifications by two separate observers (T.L. and A.S.), in a double-blind fashion.

4.3.2 Frozen sections. Fixed tissue from three cases (6, 7, and 8) (see table 4 for CC and table 7 for IG) was cryoprotected in 20% sucrose in PBS, frozen at -80 C°, and cut in 60-µm-thick serial sections on a sliding microtome from the midline for at least 0.5 cm toward the lateral portion. Sections to be used for immunohistochemistry were first transferred to a solution of 3% H_2O_2 in PBS for 30 min, to inhibit endogenous peroxidase activity, then incubated for 1 h in a blocking solution consisting of 2% BSA (Sigma) in PBS. After these steps, sections were rinsed several times in PBS and then incubated overnight at 4°C in primary anti-human nNOS policlonal antibody made in rabbit (Cayman Chemical) (Table 2) diluted 1:500 in PBS. After washing in PBS, sections were placed for 1 h at RT in a solution of bGAR secondary antibody (Vector Laboratories) (Table 3) diluted 1:200 in PBS. Sections were washed again and then reacted with a solution containing ABC complex (Vector Laboratories) diluted 1:100. After several washes, sections were processed for peroxidase histochemistry using a 0.02% solution of DAB (Sigma-Aldrich) in 0.05 mmol/L Tris buffer, pH 7.6. After a final rinse in PBS, sections were mounted on subbed slides, air-dryed, dehydrated, and then coverslipped. Immunostained sections are observed in light microscopy under a motorized Leica DM6000 microscope at different magnifications by two separate observers (T.L. and A.S.) in a double-blind fashion.

4.4 Immunofluorescence

Double labeling immunofluorescence technique was performed to define whether the nNOS positive cells found out by immunohistochemistry analysis were neurons or astrocytes. To this purpose, 5-µm thick sections from paraffin blocks were cut and transferred onto coated slides (Super Frost Plus, Menzel-Glaser, Braunschweig, Germany). Sections were deparaffinized and rehydrated via xylene and a graded series of ethyl alcohol. One section from each paraffin block was stained with Rhodamine phalloidin, (Merk S.p.a.), a high-affinity F-actin probe conjugated to the red-orange fluorescent dye tetramethylrhodamine (TRITC), in order to discriminate IG from CC with confocal microscope and to test the quality of the tissue. The first step of the immunofluorescence reaction

was the pretreatment of the sections in a water bath for 30 minutes at 90 C° in 0.1 M sodium citrate (pH 7.2), according to NeuN and GFAP datasheet. The pretreated slides were blocked for 20 minutes at room temperature with 1% BSA (Sigma) in PBS and then incubated at 4 C° overnight with different mixtures of primary antibodies (Table 2):

- anti-human nNOS policlonal antibody made in rabbit (Cayman Chemical) diluted 1:500 in PBS, and anti-human NeuN monoclonal antibody made in mouse (Merk S.p.a) diluted 1:100 in PBS, to identify nNOS positive neurons;
- anti-human nNOS policlonal antibody made in rabbit diluited 1/500 in PBS (Cayman Chemical), anti-human GFAP made in mouse diluited 1/500 in PBS (Abcam, Prodotti Gianni, Milano, Italy), to identify nNOS positive astrocytes;
- anti-human nNOS policlonal antibody made in rabbit (Cayman Chemical) diluted 1:500 in PBS, anti-human αSMA monoclonal antibody made in mouse (Agilent Dako) diluted 1:100 in PBS, and anti-human GFAP policlonal antibody made in goat (Merck S.p.a.) diluted 1:100 in PBS, to investigate the spatial relationships between nNOS positive cells and small blood vessels.

After incubation, slides were washed in PBS once and incubated in the dark for 1 hour at RT with the following secondary antibodies diluted 1:200 in PBS (Table 3): a) goat anti-rabbit IgG (Alexa fluor 488, Abcam, Cambridge, UK); b) goat anti-mouse IgG (Alexa fluor 555, Abcam) c) donkey anti-goat IgG (Alexa fluor 647, Abcam). All the sections were washed again in PBS and stained with Sudan Black to block the autofluorescence of the tissue. Finally, they were mounted in Vectashield Mounting Medium (Vector Laboratories). Fluorescence was detected with a Leica TCS-SL confocal microscope (Leica Microsystems) equipped with an Argon and He/Ne mixed gas laser. Images (pixels) were obtained sequentially from two channels using a confocal pinhole of 1.1200 and stored as TIFF files.

4.5 Quantitative analysis

Quantitative analysis of nNOS neurons was performed in IHC processed frozen sections from cases 6, 7, and 8. The number of nNOS positive cells in CC and overlying IG was counted in each section, starting from the midline towards the lateral portion of the CC. The density of neurons was expressed as number of nNOS positive neurons per mm^3. For each case, 28 sections were randomly selected (95% confidence level is used, degrees of freedom = n −1) and reproduced by means of a camera lucida attached to a Leitz Orthoplan microscope (Leitz, Wetzlar, Germany). The area of each section in mm^2 was obtained by the Image J software and the section area was multiplied by its thickness (60µm) in order to find out its volume in mm^3. The density of nNOS positive neurons was calculated only for CC because IG has a very small size and thus it was technically impossible to draw its borders by the camera lucida. In addition, in IG the distribution of nNOS positive neurons is not homogeneous, being mainly clustered around pial arterioles close to CC, and therefore we considered the calculation of neuronal density not to be so relevant.

4.6 Semiquantitative and quantitative analysis of nNOS-positive astrocytes

For the semiquantitative analysis of nNOS positive astrocyte, 11 cases from the total were selected (Table 5) and 10 paraffin sections from each subject were randomly collected and analyzed. Being the amount of astrocytes sizeable, a random sampling by the use of a frame quadrat has been used. For the quantification of nNOS and GFAP-immunopositive astrocytes, three sections 300 micrometers apart each other were analyzed for each case. Three rectangular fields were randomly analyzed for each section. The base of each rectangle measured 0.8 mm and the height was variable, being the thickness of the CC. Each rectangle was divided into squares with side of 0.8 mm, with an area of 0.64 mm^2. The count of nNOS and GFAP-positive astrocytes was performed in each square. The number of nNOS-immunopositive cells was scored with a three-point scale identifying three experimental groups and qualitatively attributed as follows: absence of cells immunopositive to

nNOS (–), few immunopositive cells (+), numerous immunopositive cells (++) (Table 6). For the graphical representation of the distribution of nNOS-positive astrocytes along the entire dorso-ventral thickness of the CC of each case, their mean number per mm^2 was calculated from all the squares located at the same dorso-ventral level in the three sections analyzed. To determine the percentage of NOS positive astrocytes versus the total number of astrocytes, the total content of nNOS and GFAP-positive astrocytes in each single rectangle was calculated by adding the counts of the squares included in the rectangle. The mean percentage was calculated across the rectan gles of the three sections of all the cases belonging to the same experimental group.

4.7 Statistical analysis

Results were expressed as mean ± standard deviation (SD) except for the distribution of nNOS positive neurons along the medio-lateral part where SD was not shown.

A two-tailed t test (PRISM software, version 4 for Windows: GraphPad Software Inc, San Diego, CA) was used to analyze and compare the data. The significance level was considered as low ($p \leq 0.05$), medium ($p \leq 0.01$) or high ($p \leq 0.001$).

4.8 Software for processing images

The brightness and contrast of the final images were adjusted using Photoshop CS6 (Adobe Systems, Mountain View, CA, USA) (RRID:SCR_014199).

5 RESULTS

5.1 Corpus callosum

5.1.1 Identification of nNOS positive neurons by light and fluorescence microscopy

To verify whether nNOS immunopositive neurons were present in the CC, immunohistochemistry was performed using the anti-nNOS antibody in paraffin sections contaninig CC; usually, paraffine sections processed also contained IG tissue, lying above the CC. To identify the CC in light microscopy, sections were treated with Luxol fast blue and eosin staining, which allowed to easily distinguished the CC from the IG (Figure 1, A, B). In sections inspected with fluorescence microscopy the Rhodamine phalloidin staining was used, evidencing in red nerve fibers, oriented in CC and IG in orthogonal fashion each other (Figure 1, C).

Neuronal NOS-positive neuronal-like cells were evident in human CC sections (Figure 2, A-H).

Double-labelling experiments by confocal microscope demonstrated that nNOS-positive neuronal-like cells in human CC are neurons, in that they showed immunopositivity both for nNOS (Figure 3, A) and NeuN (Figure 3, B), as confirmed by merging the images (Figure 3, C).

5.1.2 Morphology, distribution and quantification of nNOS–positive neurons in human CC

Neuronal NOS-positive neurons in human CC were all bipolar, showing three different morphologies: fusiform (Figure 2, A, C, H; Figure 4, Ab), ovoidal (Figure 2, D, E, G; Figure 4, Aa), and round (Figure 2, B, F; Figure 4, Ac).

The labeled neurons were generally scattered throughout the whole CC, although clusters of neurons were also observed in proximity of the boundary with IG, close to the pial arteries coming from it, and penetrating into the CC, giving rise to smaller blood vessels (bv) (Figure 5). Sometimes nNOS positive neurons in the CC seemed to establish a contact with nNOS positive neuron in the IG (Figure 4, Ac-asteresisk). The presence of numerous nNOS-positive projections fibre crossing the CC and IG was also observed (Figure 13 A-C arrowheads)

The total number, mean and percent distribution of nNOS-positive neurons in the genu, body and splenium is reported in Table 4. The body contained more nNOS neurons (55%) than the other two callosal regions (splenium 27%, genu 18%).

The mean distribution of nNOS immunopositive neurons along the medio lateral direction in the three parts of CC in the analyzed cases is shown in Figure 6. It is evident that nNOS positive neurons were more numerous at about 4 mm from the midline in the body and splenium of the CC, but were homogeneously distributed in the genu (Figure 6, A-C). The density of nNOS positive neurons in the genu, body and splenium from the three cases, expressed as the mean number of neurons per mm^3, is shown in Figure 7. The density values were statistically different among the three parts of CC and their trend was similar to that of the total number of nNOS positive neurons being the highest in the body, followed by splenium.

5.1.3 Identification of nNOS-positive astrocytes by light and fluorescence microscopy

In some autoptic samples of human CC (Table 5), immunohistochemistry showed the presence of GFAP-positive astrocytes (Figure 8 A, C, E, G) and of nNOS-positive astrocyte-like cells (Figure 8 B, D, F, H). The astrocytes were distributed over the entire CC (Figure 8, G), whereas the nNOS positive astrocytes were present especially in its boundary (Figure 8, H). When the number of nNOS positive astrocytes was high, the intensity of staining was relevant (Figure 8, B); when their number was lower, the intensity of staining was also lighter (Figure 8, D).

Double-labelling experiments showed that nNOS-positive astrocyte-like cells were immunopositive both for nNOS (Figure 9 A, C), and for GFAP (Figure 9 B, C), the specific astrocytes marker. This finding demonstrated that nNOS-positive astrocyte-like cells were actually astrocytes.

A more accurate inspection revealed a possible relationship of the nNOS astrocytes immunoreactivity with the duration of hypoxia during the lethal event. To define the hypoxia, likely influenced by the duration of the agonal time, clinical and circumstantial data have been used, as well as phone records

and witness statements. Sex, age at the time of death, agonal time lapse (as circumstantial data suggest) and postmortem-interval (PMI) were registered (Table 5).

The cases selected foresaw exclusively two classes of agonal time (At; Puccini, 2007; Scendoni et al., 2016): less than 10 minutes (short agonal time), and between 10 minutes and than 24 hours (medium agonal time); no case with agonal time that overtook the 24 hours was registered. The number of nNOS-immunopositive cells, scored with a three-point scale attributed as as described in Materials and Methods section, counted in the cases listed in Table 5, allowed us to produce the data reported in Table 6.

In cases of short duration hypoxia (agonal time less than 10 minutes), anti-nNOS antibody did not label any cell; in cases of longer hypoxia duration (agonal time from 10 minutes to 24 hours), nNOS immunopositivity appeared in astrocytes. The number of positive nNOS astrocytes was higher as the duration of the agonal time increased. Case 10 (plastic bag suffocation) gave unexpected results as it showed fewer positive nNOS astrocytes than cases 3 (drowning) and 11 (CO_2 poisoning) (see Discussion).

The ratio between the number of nNOS positive astrocytes and the number of GFAP-positive astrocytes (%) resulted significantly different ($^*p < 0.05$) in the two experimental groups where nNOS immunopositive astrocytes were present (+; ++) (Figure 10).

The quantification of nNOS positive astrocytes per mm^2 in the tissue specimens of each experimental group (+ and ++) allowed us to draw their dorsal - ventral distribution which showed the trend of a convex curve (Figure 11).

5.2 Indusium griseum

5.2.1 Western blot and identification of nNOS-positive neurons by light and fluorescence microscopy

The immunopositivity for nNOS antibody was assessed in WB using rat CC tissue lysate sample as control: the staining revealed a unique positive band at a molecular weight (160 kDa) (Figure 12, A) typical of nNOS protein. The WB of human IG lysates from fresh autoptic specimens of two cases revealed the presence of only one band at the molecular weight (160 kDa) known for nNOS (Figure 12, B, C), demonstrating the presence of this protein in the tissue.

Immunohistochemistry, performed using the anti-nNOS and anti-NeuN antibodies, showed the presence of nNOS positive neuronal-like cells (Figure 13, A-F) and of NeuN-positive neurons (Figure 13, G, H) in human IG. Neuronal NOS positive nerve fibers with dendritic spines were also frequently observed (Figure 13, A-C).

Double-labelling experiments by confocal microscope demonstrated that nNOS-positive neuronal-like cells in human IG are actually neurons, in that they showed immunopositivity both for NeuN (Figure 14, A) and nNOS (Figure 14, B), as confirmed by merging the images (Figure 14, C).

5.2.2 Morphology, distribution and quantification of nNOS–positive neurons in human IG

Neuronal NOS-positive neurons in human IG were all bipolar, showing four different morphologies: fusiform (Figure 13, E, F), rectangular (Figure 15, I), ovoidal (Figure 13, A, B, D; Figure 15, II), and round (Figure 13, C and Figure 15, III). They were present throughout the whole thickness of IG, sometimes arranged in the boundary between IG and CC (third layer of IG) (Figure 13, E, F).

Neuronal NOS-positive neurons in the IG sagittal sections were densely packed in proximity to the pial arteries penetrating into the CC, giving rise to a narrow bundle of cells and dendrites (Figure 16, B, C; Figure 17, A-F). The labeled neurons were generally clustered (Figure 16, B, C; Figure 17, C, D), although scattered neurons were also observed (Figure 17, A, B).

Neuronal NOS positive neurons were located both along rostral-caudal (Figure 16, A) and medio-lateral (Figure 18, A-C) directions. In particular, they were more numerous about 1 mm apart from the midline and their number peaks over the callosal body (63% of the total; Table 7).

Sagittal serial sections reacted with anti-nNOS and anti-α-SMA antibodies clearly evidenced the close association of neurons with vessels (Figure 17, G, H). The same close apposition of nNOS positive neurons with the wall of α-SMA positive vessels was evident in immunofluorescence reacted sections (Figure 19, D). Indeed, pial arterioles have multiple layers of smooth muscle cells and α-SMA is the actin isoform that predominates within these cells. A great number of astrocytes positive to GFAP have been observed in the IG (Figure 19, C, D, F, G), often so close to CC penetrating arterioles to give the impression that the arterioles were surrounded by astrocytic endfeet (Figure 19, G).

6. DISCUSSION

The present study describes for the first time the presence of nNOS immunopositive cells in the human adult corpus callosum and in the indusium griseum.

The double-labeling fluorescence experiments combining nNOS immunostaining with either NeuN, a neuronal marker, or GFAP, a glial marker for astrocytes, indicated that in the human CC both nNOS positive neurons and astrocytes are present; in the IG only nNOS positive neurons have been found.

6.1 NO-producing neurons in the human Corpus Callosum

The nNOS positive neurons showed a bipolar morphology, with certain heterogeneity. Following the criteria previously used on rat (Barbaresi et al., 2014), neurons found in the human CC could be classified into three main morphological groups: fusiform, ovoidal and round; this latter is the prevailing morphology of white matter neurons. The analysis of the distribution of nNOS positive neurons in human CC reveals that most intracallosal neurons seem to be scattered in dorso-ventral dimension and that some of them are located dorsally, close to IG. The distribution of nNOS-positive neurons in the CC showed a mediolateral gradient, being the cells more numerous in the lateral regions and rare in the medial region; in addition, throughout the rostrocaudal dimension, an higher density in the body and splenium was observed, and lower in the callosal genu. Comparative data on the regional distribution of nNOS-positive intracallosal neurons in primates are currently not available, in that previous study on monkeys (Rockland and Nayyar, 2012) circumscribed the analysis to the medial-most region of CC. However, the present findings are in line with previous data reported on rat (Barbaresi et al., 2014), and indicate that the adult human CC contains different neuronal populations with different areal distribution. In addition, intracallosal nNOS-positive neurons showed a wide dendritic field, with many branches extending into the white matter, some of which apparently establishing contacts with nNOS neurons in the IG. This organization is in line with a very recent paper on rat (Barbaresi et al. 2018), showing that callosal NADPH-d-positive neurons found more medially sent dendrites to the overlying IG. This close association between CC and IG neurons led

to the hypothesis that these two anatomical structures might communicate, as also suggested by the localization of nNOS neurons at the boundary between IG and CC.

6.2 NO-producing astrocytes in the human corpus callosum

This preliminary and qualitative study of a small group of cases demostrates for the first time that nNOS immunopositivity is present in CC astrocytes (Lorenzi et al., 2021), and that it may be related to hypoxia duration. Although NOS isoforms are specific of different brain cell types, in some circumstances their cellular distribution could change. Thus astrocytes, which constitutively synthesize NO mainly after calcium-independent inducible NOS expression (iNOS), by treatment with the endotoxin lipopolysaccharide (LPS) and/or certain cytokines (Merril et al., 1997), could also produce NO via the constitutive nNOS activity (Simmons and Murphy, 1992; Agulló et al., 1992). It is notable that the expression of the neuronal isoform of NOS is observed in neocortical astrocytes by spreading depression (Caggiano et al., 1998), a condition induced also by hypoxic conditions.

When hypoxia was short, nNOS immunopositivity was not observed in CC astrocytes; in case of longer hypoxia, the CC astrocytes became immunopositive to nNOS and, as the number of nNOS positive astrocytes became higher, also their labeling intensity increased. This finding is in line with a previous study performed in rat in which the number of nNOS containing neurons peaked at 4 h after focal cerebral ischemia (Zhang et al., 1994). The nNOS positivity in the astrocytes localized at the boundary of CC could represent the prompt response of these cells, positioned around the arterioles penetrating into the commissure, to the depletion of oxygen occurring during the asphyctic event preceding the death. Indeed, NO produced by astrocytes mediates vasodilation and hence the increase of blood flow to the damaged brain area. This mechanism could protect the underlying tissue against the ischemic injury. It can be hypothesized that the expression of nNOS by astrocytes in CC may be a pathophysiological brain response to hypoxia-ischemia, for reducing/preventing brain damage (Bolaños et al., 1999). It could be assumed that in the cases of short agonal time (less than

10 minutes), brain hypoxia did not occur or it was very short and with very scarce effect. In particular, in Case 10 (plastic bag suffocation), fewer positive nNOS astrocytes than cases 3 (drowning) and 11 (CO2 poisoning). According to a new recent theory, when a plastic bag is placed over the head and in close contact with the face, the sympathetic nervous system is rapidly stimulated, provoking in arrhythmias as ventricular fibrillation (Santoro et al., 2019). This latter interpretation could explain the lack of typical pathological signs of asphyxia in cases of plastic bag suffocation and therefore the fewer nNOS positive astrocytes.

In the cases of medium agonal time, hypoxia took place, able to evoke a brain tissue reaction. Alternatively, the recent observation of a direct correlation of serum GFAP with the agonal time (Breitling et al., 2018) could suggest that the increase of astrocyte nNOS immunopositivity with the hypoxia duration could be an initial event leading to an augmented astrocytic death, resulting in turn in an increased GFAP release. This hypothesis may be supported by the recent finding of the potential role of astrocytic expression of iNOS in the brain of pediatric patients in the evolution of injury following an ischemic event (Askalan et al., 2006).

Concerning the controversy about the fact that GFAP is a suitable marker to identify astrocytes, the following observations should be kept in mind: firstly, there is research arguing that the amount of GFAP in astrocytes can vary. Numerous studies demonstrated an increased amount of GFAP in reactive astrocytes in different types of lesions or in cultured astrocytes (Miyake et al., 1988; Mishima et al., 2010). Secondly, it has become clear that not all astrocytes in vivo express GFAP, or only weakly so (Mishima et al., 2010; Bushong et al., 2002; Kimelberg 2004; Giffard et al., 2005; Tatsumi et al., 2018). These studies have revealed a remarkable heterogeneity among astrocytes, the elucidation of which is ongoing (Oberheim et al., 2012; Lin et al., 2017). There is also evidence in the literature that subpopulations of astrocytes are GFAP-negative (Walz et al., 1998; Walz 2000; Kofler et al., 2002). The findings question whether the expression of GFAP is at all comparable in different astrocytes. Nevertheless, present data, evidencing a relation between the number and

labeling intensity of GFAP-labeled astrocytes and the agonal time duration, strongly suggest that such relationship could be causal.

6.3 NO-producing neurons in the human Indusium Griseum.

In the IG nNOS-positive neurons were observed, mainly clustered around pial arterioles close to CC. The nNOS-positive neurons in human IG showed a mediolateral gradient, being more numerous in the medial region and rare in the lateral regions. In addition, the number of nNOS-positive neurons is more aboundant in the IG regions overlying the callosal body than over the splenium and genu. Neuronal NOS-positive neurons found in IG displayed morphologies similar to those present in the CC, and an additional rectangular morphotype was observed. The morphological similarity between CC and IG nNOS positive neurons could suggest that some intracallosal neurons located along the dorsal callosal surface might represent heterotopic cells, displaced from indusium griseum. The same phenomenon was postulated for those neurons of CC positioned in its ventral surface which were hypothesized to come from adjacent structures such as the septohippocampal continuum and septum pellucidum (Kostovic´ et al., 2002; Milosˇevic´ and Kostovic´, 2004; Richards et al., 2004; Riederer et al., 2004; Milosˇevic´ et al., 2006; Ren et al., 2006). It is also possible that some intracallosal neurons represent a subset of neurons migrating via the corpus callosum, as already described in the rodent brain (DeDiego et al., 1994; Deng et al., 2001; Niquille et al., 2009).

The nNOS-positive neurons found in IG resemble those described by Rasonja and coworkers (2019), found in layer III of human IG, which were positive to calbindin. Since this protein has been shown to exert many functions as buffer, transporter and likely as a non-canonical sensor of Ca^{2+} (Schmidt, 2012), it is plausible that these neurons act as neural mediators of signaling between IG and CC, reciprocally enabling to be activated by other brain regions, as indicated by the presence of numerous nNOS-positive projections fibres crossing the two structures. These findings suggest that IG is not a merely rudimentary tissue (Humphrey, 1967), but likely plays a functional role in the adult brain, being actively integrated with the surrounding structures. This concept is supported by the relevant

number of astrocytes observed in the whole IG. Historically considered as merely supporting for neurons, recent research has shown that astrocytes actively participate in a large spectrum of central nervous system functions including formation, maturation and elimination of synapses, neuronal transmission and modulation of synaptic plasticity (Dallérac et al., 2016). The consistent presence of such multifunction glial cells in IG is suggestive of a very active tissue, corroborating the importance of IG in human adult brain.

6.4 Neurovascular coupling

It is known that cerebral blood flow modifies according to the functional activity of the different brain regions (functional hyperemia), so that it increases when the neural activity increases, in order to guarantee substrate and oxygen delivery and to remove the metabolism products, thus maintaining the homeostasis of the cerebral microenvironment. (Lassen et al., 1978; Raichle et al., 2006; Iadecola, 2017). The activity-induced haemodynamic response (BOLD effect) occurs when neurons, together with astrocytes and vascular cells, communicate through a complex signalling mechanism. These cells act as an integrated unit, termed the neurovascular unit, able to generate and transduce the molecular signals responsible of the changes in blood flow. Brain activation leads to the production of many vasoactive mediators (K^+, H^+, neurotransmitters and neuromodulators) which originate from neurons (including interneurons) provided with processes in close contact with blood vessels (Iadecola, 2017). Also astrocytes are involved in neurovascular regulation since they have processes in direct contact with both synapses and contractile cells of the vascular wall (Iadecola et al., 2007). In this study, the same kind of cellular organization in human IG was demonstrated, since several nNOS-positive neurons have described in close proximity to the pial arterioles penetrating into the CC, together with a great number of astrocytes, often so close to CC penetrating arterioles, that astrocytic endfeet surrounded them. It has been hypothesized that neurons, in particular nNOS-neurons, and astrocytes in close proximity of arterioles, probably form the neurovascular units of IG able to control the blood flow dorsally. Neuronal NOS-positive neurons in CC observed close to small

vessels when arterioles get deeper into the white matter exert the final fine control. Since a peculiar feature of cerebral circulation is that large cerebral arteries and pial arteries are responsible for two-thirds of the vascular resistance and therefore they are the main site of flow control (Faraci et al., 1990), it can be suggested that IG could have a crucial role in coupling local increases in blood flow of pial branches with metabolic changes related to neuronal function of the underlying CC (Milosevic et al., 2010; Sagrati et al., 2018; Sagrati et al., 2019). The prevalence of nNOS-positive neurons in the body CC and in the above IG, where information need to travel fast because crossed by sensory-motor fibers, further support the notion that these neurons are involved in modulating the blood flow in order to face the high energy demands. The corpus callosum is not an homogeneous structure since fibers connecting specific cortical areas travel throught distinct callosal regions. This topographic variability implies that there may be concomitant regional differences in terms of callosal fiber composition, as the kind of information transmitted differs across different cortical areas. Actually, the analyses of fiber composition in the primate CC reveal a wide diversity of fiber calibers, which are distributed in an uneven manner along this structure. Callosal regions connecting prefrontal and temporoparietal association areas are characterized by large proportions of poorly myelinated, small caliber, slow conducting fibers, while in regions connecting primary and secondary sensorimotor areas (callosal body) there is a concentration of fast conducting, highly myelinated fibers of more than 3 μm in diameter (Aboitiz et al., 2003). Due to their larger size, these axons have slower diffusional processes and therefore require more blood when they increase activity. Thus, it is clear the important role of nNOS neurons in the regulation of blood flow in the body of CC.

Not by chance, the long callosal artery, one of the main components of the vascular network that delivers blood to the CC, gives rise to multiple perforating branches to the CC, especially at the level of the body (Kahilogullari et al., 2008). These vessels enter the IG in the midline with a mean diameter of about 0.54 mm (range: 0,37-1.06 mm) (Kahilogullari et al., 2008) and, when they get deep in CC, become more laterally and thin. This knowledge could explain why nNOS-positive neurons counted in genu, body and splenium along their medio-lateral extension were more numerous at about 1 mm

from the midline in the IG and about 4 mm in the CC. Thus, the distribution of nNOS positive neurons in IG and CC seems to be strictly correlated to the vascular anatomy of CC so to face the increase of blood supply required by its neuronal activity.

Moreover, the nNOS immunopositivity of CC astrocytes, likely related to the duration of hypoxia, confirms the role of astrocytes in the control of CBF and provides some suggestions about the mechanism activated during an asphyxial period. Further studies will be necessary to quantify the relationship between astrocytes number, their labeling intensity and hypoxia duration. The knowledge of where and when the astrocytes become able to express nNOS could be important to understand the brain activity both under physiological and pathological conditions. A speculative hypothesis could also be advanced: very recent papers pointed out to the possibility that in some conditions the astrocytes can be reprogrammed and transformed in neurons (Qian et al., 2020; Zhou et al., 2020). The transformation could be perhaps the final step of a process triggered by a brain damage, which first leads to a proliferation of astrocytes (Ferrer-Acosta et al., 2017; Yu et al., 2020), and then to their transformation in neurons to replace the damaged cells. In this view, the nNOS expression in astrocytes after brain hypoxia could be interpreted as an early sign of the ongoing process transforming astrocytes in cells with neuronal phenotype.

In conclusion, the novel findings reported in the present thesis and summarized in Figure 20, shed new light to the interplay between CC and IG; this latter, from an undifferentiated part of the hippocampal formation, become an anatomical structure with key functional roles for the human brain, i.e. neurovascular regulation and neuronal signaling,

7. ABBREVIATIONS LIST

ABC: Avidin-Biotin-Complex

ACA: Anterior Cerebral Artery

ACoA: Anterior Communicating Artery

APA: Anterior Pericallosal Artery

BOLD: Blood Oxygen Level Dependent

BF: Blood Flow

BSA: Bovine Serum Albumin

CBF: Cerebral Blood Flow

CC: Corpus Callosum

CG: Cingulate Gyrus

DAB: 3-3' DaminoBenzidine hydrochloride

DG: Dentate Gyrus

ECM: Extra Cellular Matrix

ECL-Western blotting detection kit : Enhanced ChemiLuminescent Western blotting detection kit

EGTA: Ethylene Glycol-bis(β-aminoethyl ether)-N,N,N′,N′-TetraAcetic acid

eNOS: endothelial Nitric Oxide Synthase

fMRI: functional Magnetic Resonance Imaging

GW: Glial Wedge

GFAP: Glial Fibrillary Acidic Protein

HEPES: 4-(2-HydroxyEthyl)-1-PiperazineEthaneSulfonic acid

IG: Indusium Griseum

IGG: Indusium Griseum Glia

IgG: Immunoglobulin G

iNOS: inducible Nitric Oxide Synthase

MZG: Midline Zipper Glia

nNOS: neuronal Nitric Oxide Synthase

NO: nitric oxide

NeuN: Neuronal Nuclei

PAPA: Posterior Accessory Pericallosal Artery

PBS: Phosphate-Buffered Saline.

PCA: Posterior Cerebral Artery

PMI: Postmortem-Interval

PPA: Posterior Pericallosal Artery

RT: Room Temperature

SD: Standard Deviation

SDS-PAGE: Sodium Dodecyl Sulphate - PolyAcrylamide Gel Electrophoresis

α SMA: α-Smooth Muscle Actin

TBS: Tris-buffered saline

TBS-T: Tris-buffered saline-Tween 20

TRITC: Tetramethylrhodamine

WB: Western Blot

8. REFERENCES

- Aboitiz, F., Montiel, J. (2003). One hundred million years of interhemispheric communication: the history of the corpus callosum. *Braz J Med Biol Res*. 36: 409-420.
- Aboitiz, F., Scheibel, A.B., Fisher, R.S., Zaidel, E. (1992). Fiber composition of the human corpus callosum. *Brain Res*. 598: 143-153.
- Agulló, L., García, A. (1992). Characterization of noradrenaline - stimulated cyclic GMP formation in brain astrocytes in culture. *Biochem J.* 288: 619-624.
- Askalan, R., Deveber, G., Ho, M., Ma, J., Hawkins, C. (2006). Astrocytic-inducible nitric oxide synthase in the ischemic developing human brain. *Pediatric research.* 60: 687-92.
- Barbaresi, P., Fabri, M., Conti, F., Manzoni, T. (1987). D-[3H]aspartate retrograde labelling of callosal and association neurones of somatosensory areas I and II of cats. *J Comp Neurol.* 263:159-178.
- Barbaresi, P. (2018). Substance P receptor in the rat indusium griseum during postnatal development. *Neurosci Res*. 130: 23-38.
- Barbaresi, P., Fabri, M., Mensà, E. (2014). Characterization of NO producing neurons in the rat corpus callosum. *Brain Behav*. 4: 317- 336.
- Bolaños, J.P., Almeida, A. (1999). Roles of nitric oxide in brain hypoxia-ischemia. *Biochim Biophys Acta*. 1411: 415-436.
- Breitling, B., Brunkhorst, R., Verhoff, M., Foerch, C. (2018). Post-mortem serum concentrations of GFAP correlate with agony time but do not indicate a primary cerebral cause of death. *PLoS One*. 13: e0205323.
- Buskila Y, Farkash S, Hershfinkel M, Amitai Y. (2005). Rapid and reactive nitric oxide production by astrocytes in mouse neocortical slices. *Glia.* 52: 169-176.
- Bushong, E.A., Martone, M.E., Jones, Y.Z., Ellisman, M.H. (2002). Protoplasmic astrocytes in ca1 stratum radiatum occupy separate anatomical domains. *J Neurosci*. 22: 183–192.
- Caggiano, A.O., Kraig, R.P. (1998). Neuronal nitric oxide synthase expression is induced in neocortical astrocytes after spreading depression. *J Cereb Blood Flow Metab*. 18: 75-87.
- Cinelli, M.A., Do, H.T., Miley, H.P., Silverman, R.B. (2019). Inducible nitric oxide synthase: Regulation, structure, and inhibition. *Med Res Rev*. 1-32.
- Cohn, E.H., Sacks. E.J., Heymann, M.A., Rudolph, A.M., (1974). Cardiovascular responses to hypoxemia and acidemia in fetal lambs. *Am J Obstet Gynecol*. 120: 817-822.
- Dallérac, G., Rouach, N. (2016). Astrocytes as new targets to improve cognitive functions. *Prog Neurobiol*. 144: 48-67

- Dawson, T.M., Snyder, S.H. (1994). Gases as biological messengers: nitric oxide and carbon monoxide in the brain. *J Neurosci.* 14: 5147-5159.
- DeDiego, I., Smith-Fernandez, A., Fairen, A. (1994) Cortical cells that migrate beyond area boundaries: characterization of an early neuron population in the lower intermediate zone of prenatal rats. *Eur J Neurosci*. 6: 983-997.
- Deng, J., Elberger, A.J. (2001). The role of pioneer neurons in the development of mouse visual cortex and corpus callosum. *Anat Embryol.* 204: 437-453.
- Deoni, S.C., Mercure, E., Blasi, A., Gasston, D., Thomson, A., Johnson, M., Williams, S.C., Murphy, D.G. (2011). Mapping infant brain myelination with magnetic resonance imaging. *J Neurosci*. 31: 784 -791.
- Di Ieva, A., Tschabitscher, M., Rodriguez, Y., Baena, R. (2007). Lancisi's nerves and the seat of the soul. *Neurosurgery*. 60: 563-568.
- Di Ieva, A., Fathalla, H., (2015). The indusium griseum and the longitudinal striae of the corpus callosum. *Cortex*. 62: 34-40.
- Estrada, C., DeFelipe, J. (1998). Nitric oxide-producing neurons in the neocortex: morphological and functional relationship with intraparenchymal microvasculature. *Cereb Cortex*. 8:193-203.
- Fabri, M., Manzoni, T. (2004). Glutamic acid decarboxylase immunoreactivity in callosal projecting neurons of cat and rat somatic sensory areas. *Neuroscience.* 123: 557-566.
- Fabri, M., Pierpaoli, C., Barbaresi, P., Polonara, G. (2014). Functional topography of the corpus callosum investigated by DTI and fMRI. *World J Radiology*. 6: 895- 906.
- Fabri, M., Polonara, G. (2013). Functional topography of the human corpus callosum: an fMRI mapping study. *Neural Plast*. doi: 10.1155/2013/251308.
- Fabri, M., Polonara, G., Mascioli, G., Salvolini, U., Manzoni, T. (2011). Topographical organization of human corpus callosum: an fMRI mapping study. *Brain Res*. 1370: 99-111.
- Fantini, S., Sassaroli, A., Tgavalekos, K.T., Kornbluth, J. (2016). Cerebral blood flow and autoregulation: current measurement techniques and prospects for noninvasive optical methods. *Neurophotonics*. 3: 031411.
- Faraci, F.M., Heistad, D.D. (1990). Regulation of large cerebral arteries and cerebral microvascular pressure. *Circ Res*. 66: 8-17.
- Ferrer-Acosta, Y., Gonzalez-Vega, M.N., Rivera-Aponte, D.E., Martinez-Jimenez, S.M., Martins, A.H. (2017). Monitoring Astrocyte Reactivity and Proliferation in Vitro Under Ischemic-Like Conditions. *J Vis Exp*. 128: 55-108. doi:10.3791/55108.

- Gawryluk, J.R., Mazerolle, E.L., D'Arcy, R.C. (2014). Does functional MRI detect activation in white matter? A review of emerging evidence, issues, and future directions. *Front Neurosci.* 8: 239.
- Gazzaniga, M. S. (2000). Cerebral specialization and interhemispheric communication: does the corpus callosum enable the human condition? *Brain* 123: 1293-1326.
- Giffard, R.G., Swanson, R.A. (2005). Ischemia-induced programmed cell death in astrocytes. *Glia.* 50: 299–306.
- Higo, S., Akashi, K., Sakimura, K., Tamamaki, N. (2009). Subtypes of GABAegic neurons project axons in the neocortex. *Front Neuroanat.* 3:25.
- Ho, J.J., Man, H.S., Marsden, P.A. (2012). Nitric oxide signaling in hypoxia. *J Mol Med*. 90:217-231.
- Humphrey, T. (1967). The development of the human hippocampal fissure. *J Anat.* 101: 655-676.
- Iadecola, C., Nedergaard, M. (2007). Glial regulation of the cerebral microvasculature. Nat *Neurosci.* 10: 1369-1376.
- Iadecola, C. (2004). Neurovascular regulation in the normal brain and in Alzheimer's disease. *Nat Rev Neurosci*. 5: 347-360.
- Iadecola, C. (2017). The neurovascular unit coming of age: a journey through neurovascular coupling in health and disease. *Neuron*. 96: 17-42.
- Innocenti, G. M. (1986). General organization of callosal connections in the cerebral cortex. 291-353.
- Kahilogullari, G., Ugur, H.C., Comert, A., Tekdemir, I., Kanpolat, Y. (2012). The branching pattern of the middle cerebral artery: is the intermediate trunk real or not? An anatomical study correlating with simple angiography. *J Neurosurg*. 116(5):1024-34. doi: 10.3171/2012.1.JNS111013.
- Kahilogullari, G., Comert, A., Arslan, M., Esmer, A.F. (2008). Callosal branches of the anterior cerebral artery: an anatomical report. *Clin Anat*. 21: 383-388.
- Kakou, M., Destrieux, C., Velut, S. (2000). Microanatomy of the pericallosal arterial complex. *J Neurosurg*. 93: 667-675.
- Kimelberg, H.K. (2004). The problem of astrocyte identity. *Neurochem. Int*. 45:191–201.
- Kofler, B., Bulleyment, A., Humphries, A., Carter, D.A. (2002). Id-1 expression defines a subset of vimentin/s-100ß-positive, gfap-negative astrocytes in the adult rat pineal gland. *Histochem J.* 34: 167–171.
- Kostovic´, I., Rasˇin, M., Petanjek, Z., Judasˇ, M. (2002) Morphological characteristics of the cells in the subcallosal zone (nucleus septohippocampalis) of the human fetus. *Neuroembryology*. 1: 97-104.

- Laranjinha, J., Santos, R.M., Lourenc, ´ C.F. (2012). Nitric oxide signaling in the brain: translation of dynamics into respiration control and neurovascular coupling. *Ann NY Acad Sci.* 1259:10-8.
- Lassen, N.A., Ingvar, D.H., Skinhøj, E. (1978). Brain function and blood flow. *Sci Am*. 239: 62-71.
- Lauritzen, M. (2005). Reading vascular changes in brain imaging: is dendritic calcium the key? *Nat Rev Neurosci.* 6:77-85.
- Lin, C.J., Yu, K., Hatcher, A., Huang, T., Lee, H., Carlson, J., Weston, M.C., Chen, F., Zhang, Y., Zhu, W. (2017). Identification of diverse astrocyte populations and their malignant analogs. *Nat. Neurosci.* 20: 396–405.
- Logothetis, N.K., Pauls, J., Augath, M., Trinath, T., Oeltermann, A. (2001). Neurophysiological investigation of the basis of the fMRI signal. *Nature*; 412: 150-157.
- Lorenzi, T., Sagrati, A., Montanari, E., Tagliabracci, A., Barbaresi, P., Fabri, M., Morroni, M. (2019). Letter: The Indusium Griseum: anatomic study with potential application to callosotomy. *Neurosurgery.* 85:621-622.
- Lorenzi, T., Graciotti, L., Sagrati, A., Reguzzoni, M., Protasoni, M., Minardi, D., Milanese, G., Cremona, O., Fabri, M., Morroni, M. (2020). Normal human macula densa morphology and cell turnover: A histological, ultrastructural, and immunohistochemical investigation. *The Anatomical Record*. doi: 10.1002/ar.24465.
- Lorenzi, T., Sagrati, A., Montanari, E., Senzacqua, M., Morroni, M., Fabri, M. (2021). Hypoxia-induced expression of neuronal nitric oxide synthase in astrocytes of human corpus callosum. *Brain Struct Funct*. doi: 10.1007/s00429-021-02244-5.
- Malobabić, S. (1982). Morfologija, topografija i građa corpus callosum-a. Doktorska disertacija. Univerzitet u Beogradu, Medicinski fakultet. Beograd.
- Malobabic', S., Bogdanovic′ , D., Drekic, D. (1984). On the neurons with dendrites intermingling with the fibers of the human corpus callosum: a Golgi picture. *Gegenbaurs Morph Jahrb*. 130:557-564.
- Mazerolle, E.L., D'Arcy, R.C., Beyea. S.D. (2008). Detecting functional magnetic resonance imaging activation in white matter: interhemispheric ransfer across the corpus callosum. *BMC Neurosci*. 9: 84.
- Meldrum, B.S. (2000). Glutamate as a neurotransmitter in the brain: review of physiology and pathology. *J Nutr.* 13:1007-1015.

- Merrill, J.E., Murphy, S.P., Mitrovic, B., Graham, M.A., Dopp, J.C., Ding, M., Griscavage, J., Ignarro, L.J., Lowenstein, C.J. (1997). Inducible nitric oxide synthase and nitric oxide production by oligodendrocytes. *J Neurosci Res*. 48:372-384.
- Miyake, T., Hattori, T., Fukuda, M., Kitamura, T., Fujita, S. (1988). Quantitative studies on proliferative changes of reactive astrocytes in mouse cerebral cortex. *Brain Res*. 451:133–138.
- Milosˇevic´, J.N., Petanjek, Z., Petrovic, D., Judas, M., Kostovic, I. (2010). Morphology, molecular phenotypes and distribution of neurons in developing human corpus callosum. *Eur J Neurosci*. 32:1423-1432.
- Milosˇevic´, N.J., Benjak, V., Kostovic´, I. (2006) Transient cellular structures in developing corpus callosum of the human brain. *Coll Antropol*. 30: 375–381.
- Milosˇevic´, N.J., Kostovic´, I. (2004) Immunohistochemical characterization of midline cellular structures associated with growing corpus callosum in human fetus. FENS Abstr., 2, A146.10.
- Mishima, T., Hirase, H. (2010). In vivo intracellular recording suggests that gray matter astrocytes in mature cerebral cortex and hippocampus are electrophysiologically homogeneous. *J Neurosci.* 30:3093–3100.
- Niquille, M., Garel, S., Mann, F., Hornung, J.P., Otsmane, B., Chevalley, S., Parras, C., Guillemot, F., Gaspar, P., Yanagawa, Y. & Lebrand, C. (2009) Transient neuron populations are required to guide callosal axons: a role for semaphorin 3C. doi: PLoS Biol., 7, e1000230.
- Oberheim, N.A., Goldman, S.A., Nedergaard, M. (2012). Heterogeneity of astrocytic form and funktion. *Methods Mol. Biol*. 814:23–45.
- Perrenoud, Q., Rossier, J., Férézou, I., Geoffroy, H., Gallopin, T., Vitalis, T., Rancillac, A. (2012). Activation of cortical 5-HT3 receptor-expressing interneurons induces NO mediated vasodilatations and NPY mediated vasoconstrictions. *Front Neural Circuits*. 6:50.
- Petzold, G.C., Murthy, V.N. (2011). Role of astrocytes in neurovascular coupling. *Neuron* 71:782-797.
- Polonara, G., Mascioli, G., Foschi, N., Salvolini, U., Pierpaoli, C., Manzoni, T., Fabri, M., Barbaresi, P. (2014). Further evidence for the topography and connectivity of the corpus callosum: an fMRI study of patients with partial callosal resection. *J Neuroimaging*. doi: 10.1111/jon.12136.
- Provenzale, J.M., Isaacson, J., Chen, S. (2012). Progression of corpus callosum diffusion-tensor imaging values during a period of signal changes consistent with myelination. *AJR Am J Roentgenol*. 198: 1403-1408.
- Puccini, C. (2007). Istituzioni di Medicina Legale. CEA, Milano

- Qian, H., Kang, X., Hu, J., Zhang, D., Liang, Z., Meng, F., Zhang, X., Xue, Y., Maimon, R., Dowdy, S.F., Devaraj, N.K., Zhou, Z., Mobley, W.C., Cleveland, D.W., Fu, X.D. (2020). Reversing a model of Parkinson's disease with in situ converted nigral neurons. *Nature*. 582: 550-577.
- Raichle, M.E., Mintun, M.A. (2006). Brain work and brain imaging. *Annu Rev Neurosci.* 29: 449-476.
- Rakic, P., Yakovlev P. I. (1968). Development of the corpus callosum and cavum septi in man. *J Comp Neurol*, 132:1.
- Rasonja, B.M., Oreškovi´, D., Knezovi´, V., Pogledi´, I., Pupaˇci´, D., Vukši, M., Brugger, P.C., Prayer, D., Petanjek, Z., Miloševi´c, N. M. (2019). Histological and mri study of the development of the human indusium griseum. *Cereb Cortex.* 29: 4709-4724.
- Raybaud, C. (2010). The corpus callosum, the other great forebrain commissures, and the septum pellucidum: anatomy, development, and malformation. *Neuroradiology*. 52: 447-477.
- Ren, T., Anderson, A., Shen, W. B., Huang, H., Plachez, C., Zhang, J., Mori, S., Kinsman, S.L., Richards, L.J. (2006) Imaging, anatomical, and molecular analysis of callosal formation in the developing human fetal brain. *Anat Rec A Discov Mol Cell Evol Biol*. 288: 191-204.
- Revich, M., Brann, A.W. Jr., Shapiro, H., Myers, R.E. (1972) Regional cerebral blood low during prolonged partial asphyxia. In: Meyer JS, Revich M, Lechner H, Eichorn O (eds) Research on the Cerebral Circulation. Fifth International Salzburg Conference, Charles C. Thomas, Springfield, IL, 216-227.
- Revishchin, A. V., Okhotin, V. E., Korochkin L. I., Pavlova G. V. (2010). A new population of calretinin-positive cells, presumptively neurons, with polymorphous spines in the mouse. *Forebrain Neuroscience and Behavioral Physiology*. 40: 541–552.
- Richards, L. J., Planchez, C., Ren, T. (2004). Mechanisms regulating the development of the corpus callosum and its agenesis in mouse and human. *Clinical Genetics*. 66: 276-89.
- Riederer, B.M., Berbel, P., Innocenti, G.M. (2004). Neurons in the corpus callosum of the cat during postnatal development. *Eur J Neurosci*, 19: 2039- 2046.
- Rockland, K.S., Nayyar, N. (2012). Association of type I neurons positive for NADPH-diaphorase with blood vessels in the adult monkey corpus callosum. *Front Neural Circuits.* 6:4 doi:10.3389/fncir.2012.00004.
- Sagrati, A., Lorenzi, T., Sagrati, A., Montanari, E., Tagliabracci, A., Barbaresi, P., Fabri, M., Morroni, M. (2019). Quantification and characterization of nitric oxide neurons in human corpus callosum. In: Joint Meeting of the Federation of European Physiological Societies (FEPS) and the Italian Physiological Society (SIF), Bologna, September 10-13, Italy.

- Sagrati, A., Lorenzi, T., Montanari. E., Tagliabracci. A., Barbaresi, P., Morroni, M., Fabri, M. (2018). Morfological and neurochemical analysis of the human corpus callosum. 69th Congress of the Physiological Society of Italy (SIF 2018), Firenze, September 19-21.
- Santoro, P., La Russa, R., Besi, L., Voloninno, G., dell'Aquila, M., De Matties, A., Maiese, A. (2019). The forensic approach to plastic bag suffocation: Case reports and review of the literature. *Med Leg J.* 87:214-220.
- Scendoni, R., Ferrante, L., Stramazzotti, D., Tagliabracci, A. (2016). Analysis of immunohistochemical expression of inducible nitric oxide synthase for the evaluation of agonal time in forensic medicine. Int J Legal Med. 130(6):1639-1646. doi: 10.1007/s00414-016-1402-8.
- Schmidt, H. (2012). Three functional facets of calbindin D-28k. *Front Mol Neurosci*. 5: 25.
- Shu, T., Sundaresan, V., Mccarthy, M. M., Richards, L. J. (2003). Slit2 guides both precrossing and postcrossing callosal axons at the midline in vivo. *J Neurosci*. 23: 8176-8184.
- Silver, J., Edwards, M. A., Levitt, P. (1993). Immunocytochemical demonstration of early appearing astroglial structures that form boundaries and pathways along axon tracts in the fetal brain. *J Comp Neurol.* 328: 415-36.
- Simic´, G., Lucassen, P. J., Krsnik, Z., Krusˇlin, B., Kostovic´I., Winblad, B., Bogdanovic, N. (2000). nNOS Expression in Reactive Astrocytes Correlates with Increased Cell Death Related DNA Damage in the Hippocampus and EntorhinalCortex in Alzheimer's Disease. *Experimental Neurology.* 165: 12–26.
- Simmons, M.L., Murphy, S. (1992). Induction of nitric oxide synthase in glial cells. *J Neurochem*. 59:897-905.
- Standring, S., Gray, H. (2008). Gray's anatomy: The anatomical basis of clinical practice. Edinburgh: Churchill Livingstone/Elsevier.
- Sturrock, R.R. (1977). Quantitative and morphological changes in neurons and neuroglia in the indusium griseum of aging mice. *J Gerontol*. 32: 647-658.
- Sturrock, R.R. (1978a). Development of the indusium griseum. III. An autoradiographic study of cell production. *J Anat*. 126:1-6.
- Sturrock, R.R. (1978b). Development of the indusium griseum. II. A semithin light microscopic and electron microscopic study. *J Anat*. 125: 433-445.
- Sturrock, R.R. (1978c). Development of the indusium griseum. I. A quantitative light microscopic study of neurons and glia. *J Anat*. 125: 293-298.
- Tatsumi, K., Isonishi, A., Yamasaki, M., Kawabe, Y., Morita-Takemura, S., Nakahara, K., Terada, Y., Shinjo, T., Okuda, H., Tanaka, T. (2018). Olig2-lineage astrocytes: a distinct subtype of

astrocytes that differs from gfap astrocytes. *Front Neuroanat*. 12, 8.

- Tettamanti, M., Paulesu, E., Scifo, P., Maravita, A., Fazio, F., Perani, D., Marzi, C.A. (2002). Interhemispheric transmission of visuomotor information in humans: fMRI evidence. *J Neurophysiol*. 88: 1051-1058.
- Türe, U., Yaşargil, M. G., Krisht, A. F. (1996). The Arteries of the corpus callosum: a microsurgical anatomic study. *Neurosurgery*. 39: 1075–1084. doi.org/10.1097/00006123-199612000-00001.
- Ugur, H.C., Kahilogullari, G., Esmer, A.F., Comert, A., Odabasi, A.B., Tekdemir, I., Elhan, A., Kanpolat, Y. (2006). A Neurosurgical View of Anatomical Variations of the Distal Anterior Cerebral Artery: An Anatomical Study. *J Neurosurg* .104: 278-284.
- Walz, W., Lang, M.K. (1998). Immunocytochemical evidence for a distinct gfap-negative subpopulation of astrocytes in the adult rat hippocampus. *Neurosci Lett*. 257: 127–130.
- Walz, W. (2000). Controversy surrounding the existence of discrete functional classes of astrocytes in adult gray matter. *Glia*. 31: 95–103.
- Watanabe, M., Maemura, K., Kanbara, K., Tamayama, T., Hayasaki, H. (2002). GABA and GABA receptors in the central nervous system and other organs. *Int Rev Cytol.* 213:1-47.
- Wood, J., Garthwaite J. (1994). Models of the diffusional spread of nitric oxide: implications for neural nitric oxide signalling and its pharmacological properties. *Neuropharmacology*. 33:1235-44.
- Wyss, J.M., Sripanidkulchai, K. (1983). The indusium griseum and anterior hippocampal continuation in the rat. *J Comp Neurol*. 219: 251-272
- Yu, X., Nagai, J., Khakh, B.S. (2020). Improved tools to study astrocytes. *Nat Rev Neurosci.* 21:121-138.
- Zhang, J., Snyder, S.H. (1995). Nitric oxide in the nervous system. *Annu Rev Pharmacol Toxicol*. 35:213-233.
- Zhang, Z.G., Chopp, M., Gautam, S., Zaloga, C., Zhang, R.L., Schmidt, H.H., Pollock, J.S., Förstermann, U. (1994). Upregulation of neuronal nitric oxide synthase and mRNA, and selective sparing of nitric oxide synthase-containing neurons after focal cerebral ischemia in rat. *Brain Res.* 654:85-95
- Zhou, H., Su, J., Hu, X., Zhou C., Li, H., Chen, Z., Xiao, Q., Wang, B., Wu, W., Sun, Y, Zhou, Y., Tang, C., Liu, F., Wang, L., Feng, C., Liu, M., Li, S., Zhang, Y., Xu, H., Yao, H., Shi, L., Yang, H. (2020). Glia-to-Neuron Conversion by CRISPR-CasRx Alleviates Symptoms of Neurological Disease in Mice. *Cell.* 181:590-603.
- Ziskin, J.L., Nishiyama, A., Rubio, M., Fukaya, M., Bergles, D.E. (2007). Vesicular release of glutamate from unmyelinated axons in white matter. *Nat Neurosci.* 10:321-330.

9. FIGURES

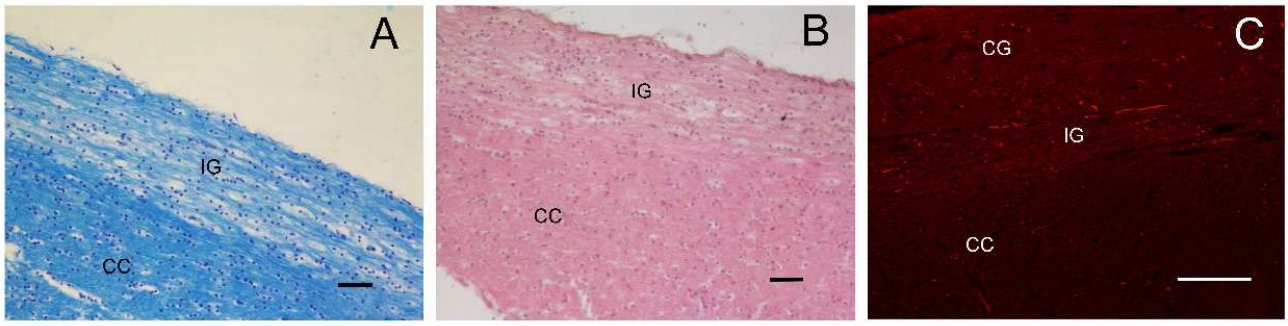

FIGURE 1

Photomicrographs in light microscopy of a sagittal section of callosal genu stained by Luxol fast blue (A) and eosin (B); (C), photomicrograph in fluorescence microscopy of a genu sagittal section stained with Rhodamine phalloidin. Calibration bars: 50 µm in A and B, 100 µm in C.

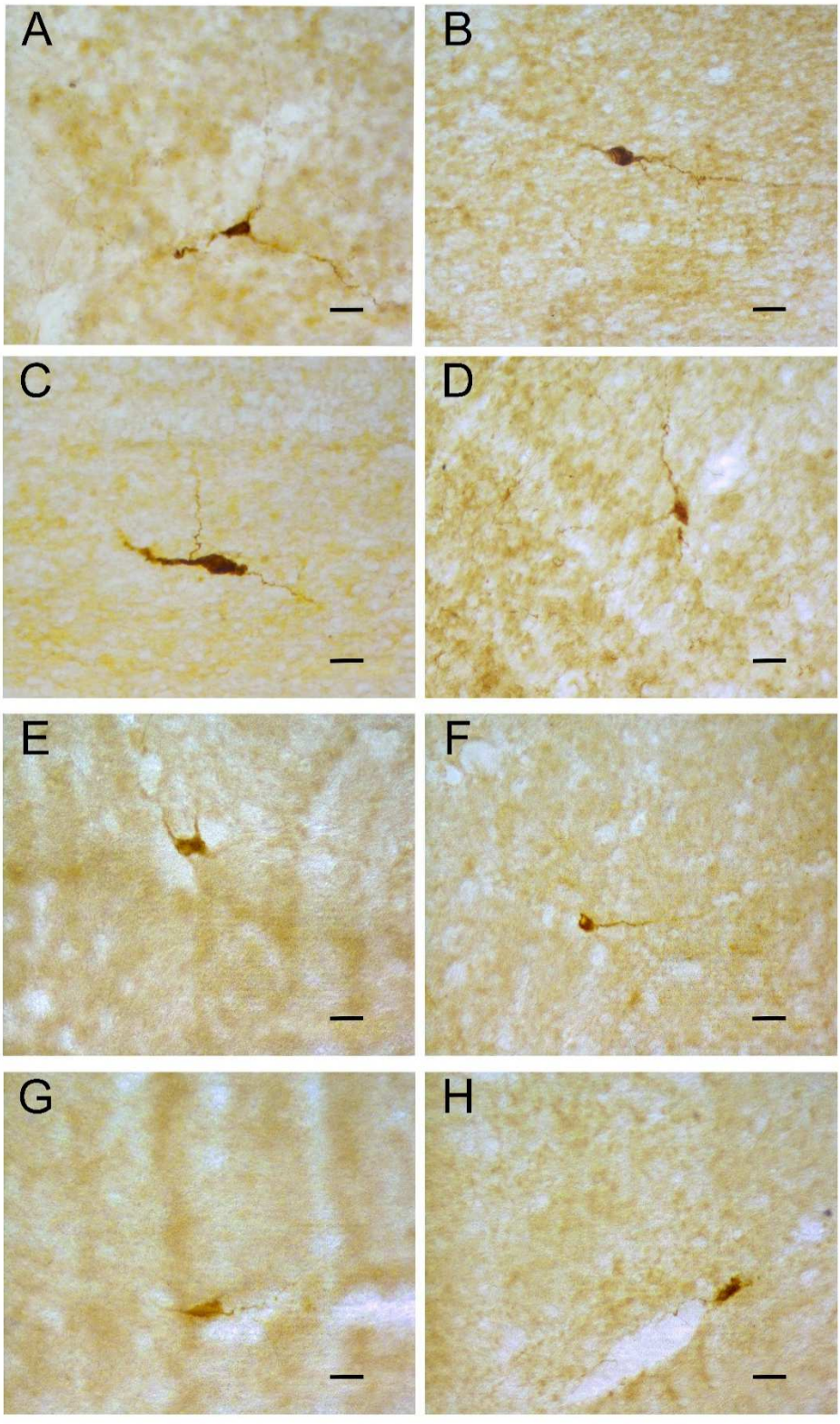

FIGURE 2

Photomicrographs of nNOS-immunopositive neurons in sagittal sections from human callosal genu. Different morphological types of nNOS immunopositive cells are evident: fusiform (A, C, H), ovoidal (D, E, G), round (B, F). All these cells are bipolar and horizontally oriented. Calibration bars: 25 µm.

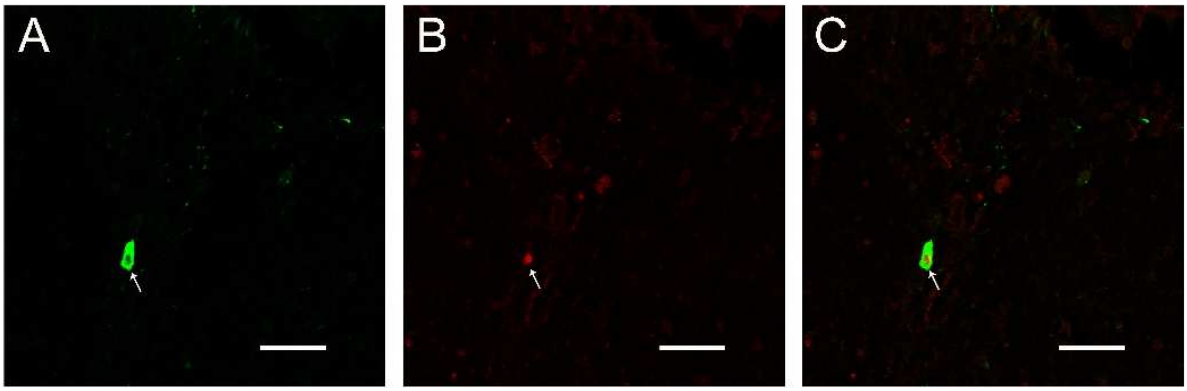

FIGURE 3

Confocal laser scanning photomicrographs of human genu. A, a nNOS positive cell (green), (arrow); B, a cell positive to NeuN (red) (arrow); C, merged images, showing that the cells in A and in B are the same neuron. Calibration bars: 100 μm.

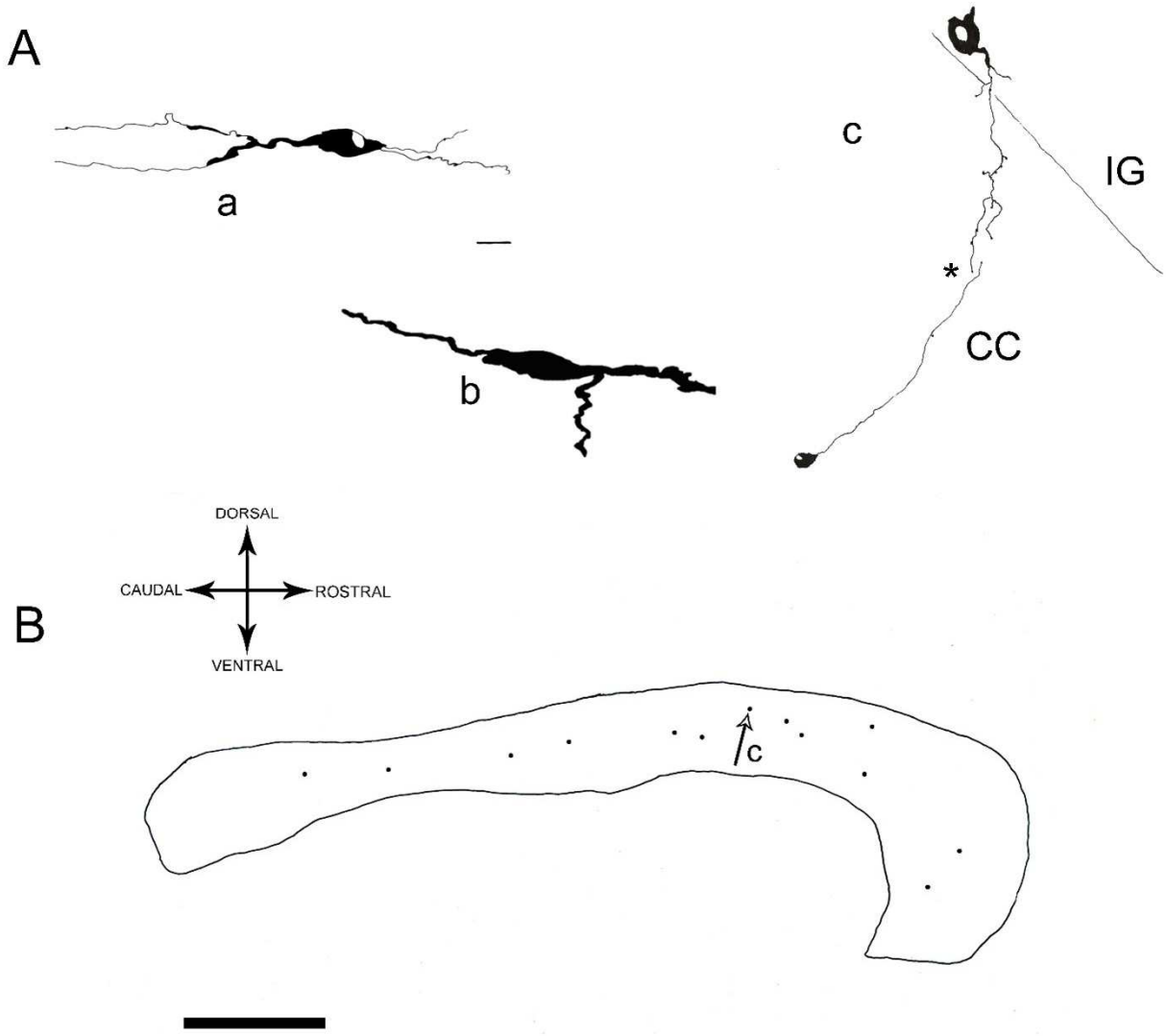

FIGURE 4

Camera lucida drawings of nNOS-immunopositive neurons in the human CC. A: three morphological types (a) ovoidal; (b) fusiform, (c) round. B, distribution of nNOS-positive neurons in the whole CC; one region is indicated (c, arrows) enlarged in c (40x), where IG neurons is close to CC neuron and seem to establish a contact between them (asterisk). Calibration bars: A 10 µm; B, 1 cm.

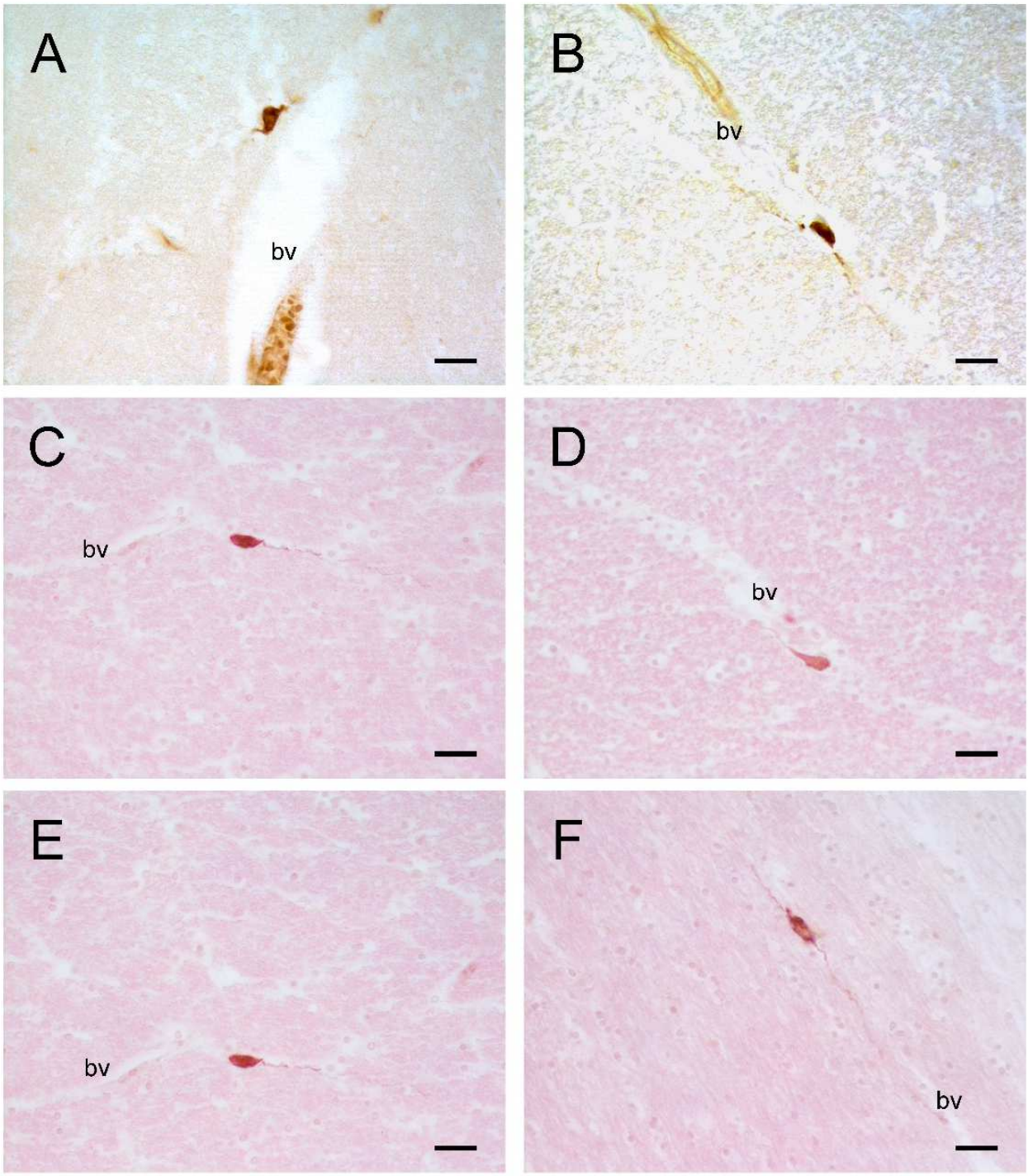

FIGURE 5

Photomicrographs showing nNOS-positive neurons close to blood vessels (bv), in eosin counterstained sections. Calibration bars: 25 µm.

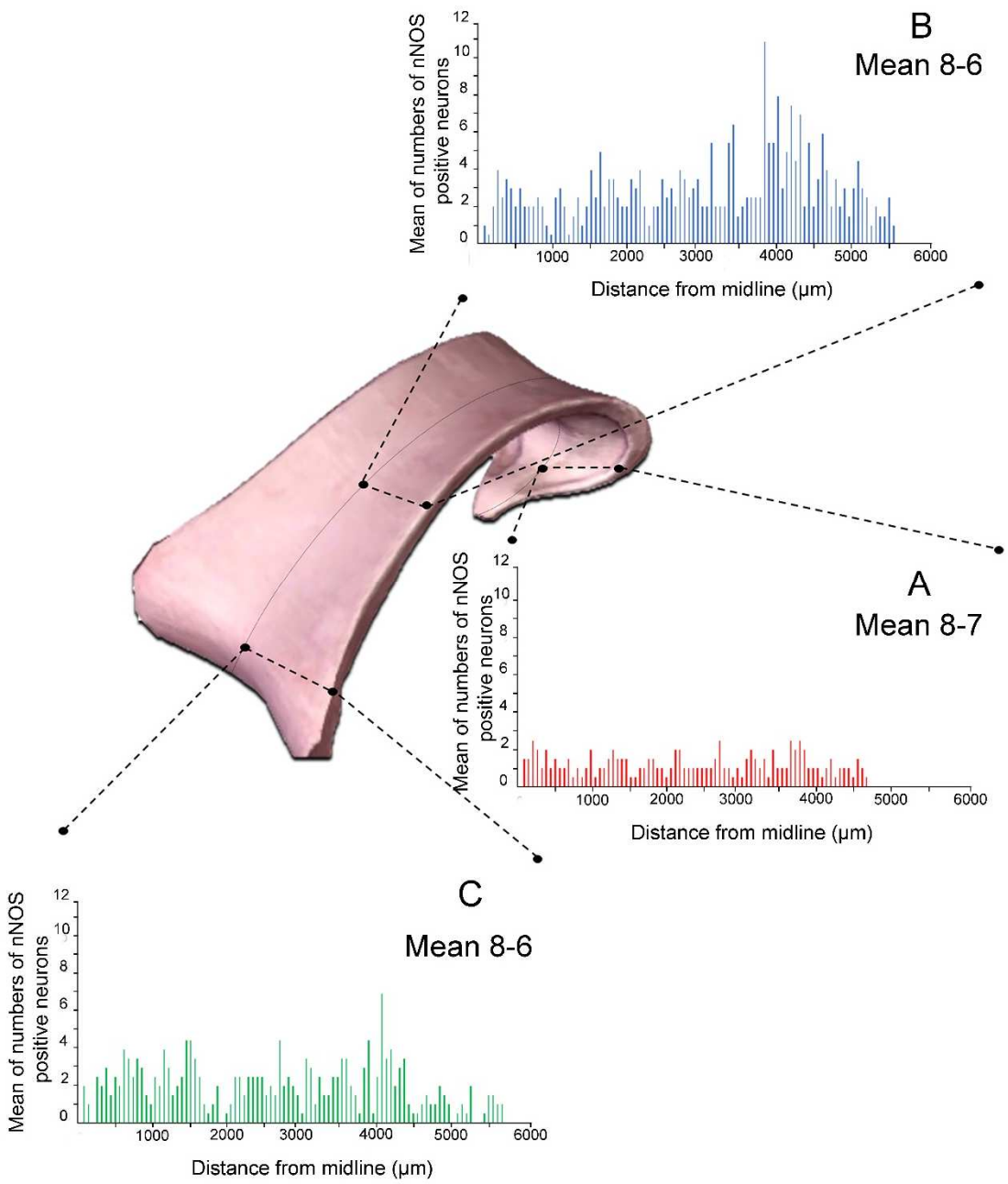

FIGURE 6

Graphs reporting the mean distribution of nNOS-immunopositive neurons along the whole human CC from three cases (6, 7, and 8, right hemisphere): neurons counted along the medio-lateral dimension in the callosal genu (A), callosal body (B), and callosal splenium (C).

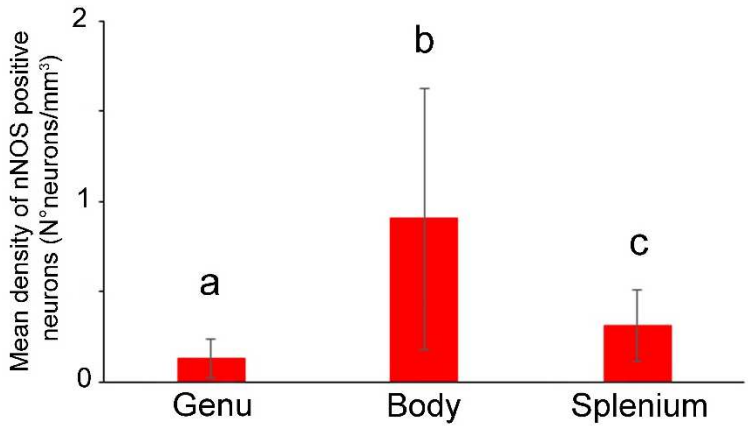

FIGURE 7

Graph showing the mean density of nNOS-positive neuron in the three callosal regions (genu, body and splenium) in cases 6, 7 and 8, expressed as number of neurons per mm^3. Different letters indicate statistically significant differences among experimental groups. Genu vs body (P = 0.0001); genu vs splenium (P = 0.0001); body vs splenium (P = 0.0001).

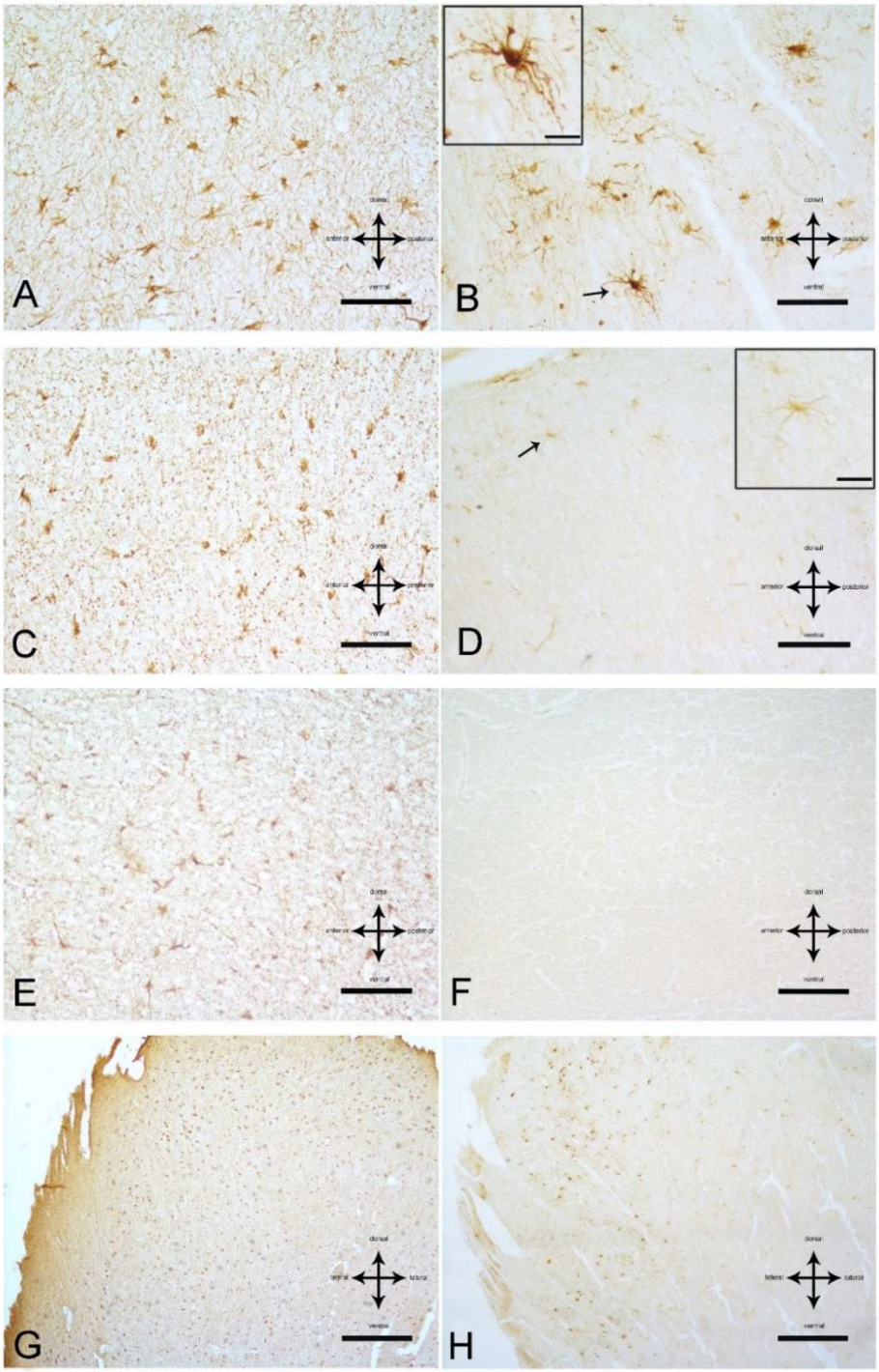

FIGURE 8

GFAP-positive astrocyte cells (A, C, E) and nNOS-positive astrocyte-like cells (B, D, F) in three subjects with different hypoxia duration: A and B from case 3 (++); C and D from case 6 (+); E and F from case 2 (-). The inserts in frames B and D show nNOS-positive astrocyte-like cells (arrows) at higher magnification. GFAP-positive astrocyte cells are homogeneously distributed in the CC (G); nNOS-positive astrocyte-like cells are located close to the CC boundary (H). A-F, sagittal sections; G, H, coronal sections. Calibration bars: 100 µm in A-F; 500 µm in G, H; 25 µm in the inserts.

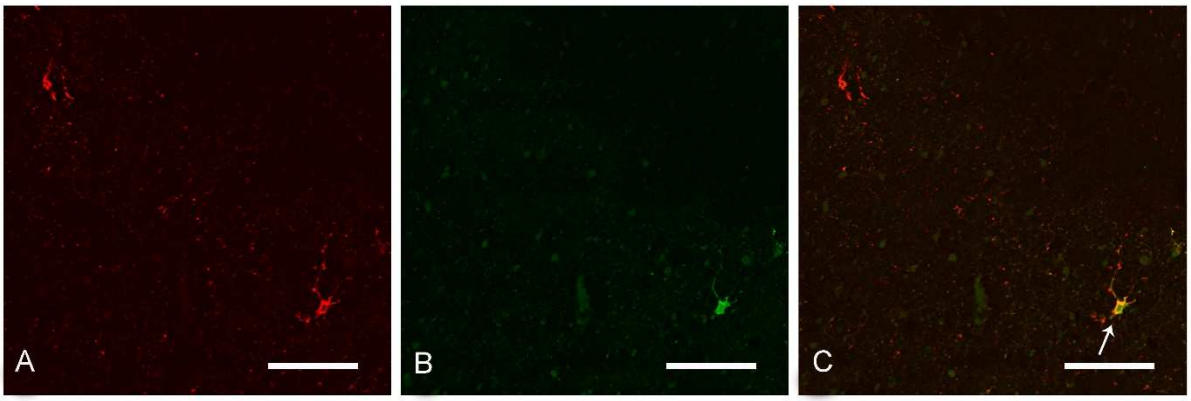

FIGURE 9

Confocal laser scanning photomicrographs. A, GFAP-positive astrocytes (red); B, nNOS-positive astrocyte-like cell (green); C, merged image: the yellow cell (arrow) is an nNOS-positive astrocyte. Calibration bar: 75 µm.

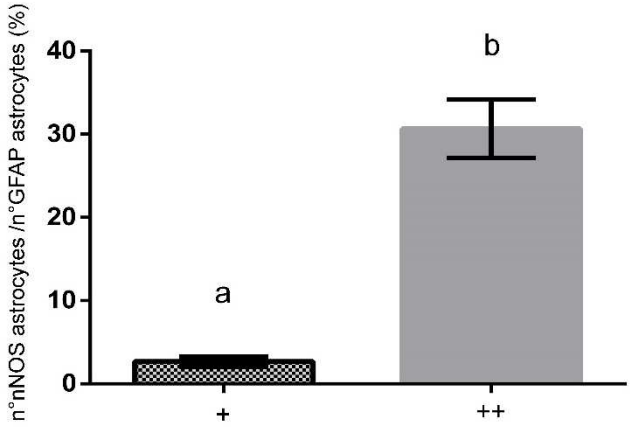

FIGURE 10

Ratio between the number of nNOS-positive astrocytes and the number of GFAP-positive astrocytes (%) in two experimental groups (+; ++). Data shown are mean (M) ± standard deviation (SD). Letters indicate statistically significant differences ($p < 0.05$) between experimental groups. Different letters indicate statistically significant differences among experimental groups. + vs ++ (P = 0.0002).

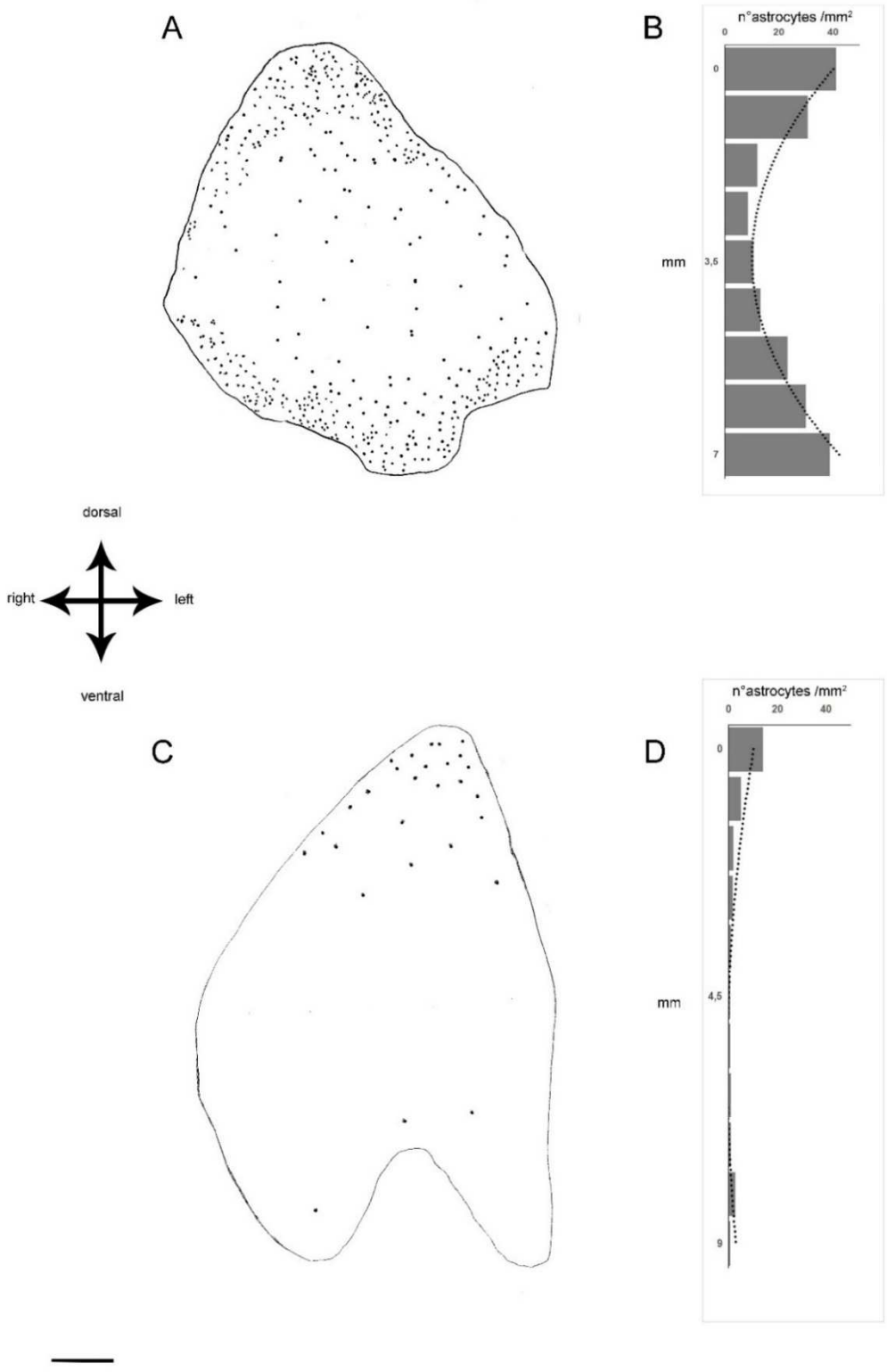

FIGURE 11

Dorso-ventral distribution of nNOS-positive astrocytes in one representative specimen of each experimental group. A, C camera lucida representation of the coronal section of genu from subject 3 (++) and subject 7 (+), respectively. B, D histograms showing the numbers of nNOS astrocytes per mm^2 from dorsal to ventral side (mm) obtained by the counts of astrocytes in three sections of genu from subject 3 (++) and subject 7 (+) (trend line R^2 =0.9267 and R^2 =0.7561, respectively). Calibration bar: 1 mm.

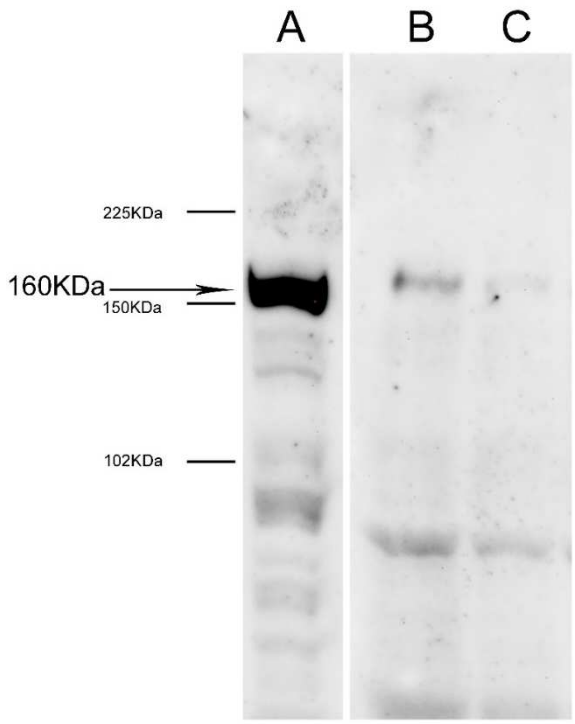

FIGURE 12

Cropped Western Blot image showing the presence of nNOS-immunoreactivity in the human IG. A, rat CC as control; B and C, human IG tissue lysates from two cases (10, 11) on 8% SDS-polyacrilamide gel. The detected band shows the molecular weight of 160 kDa expected for nNOS.

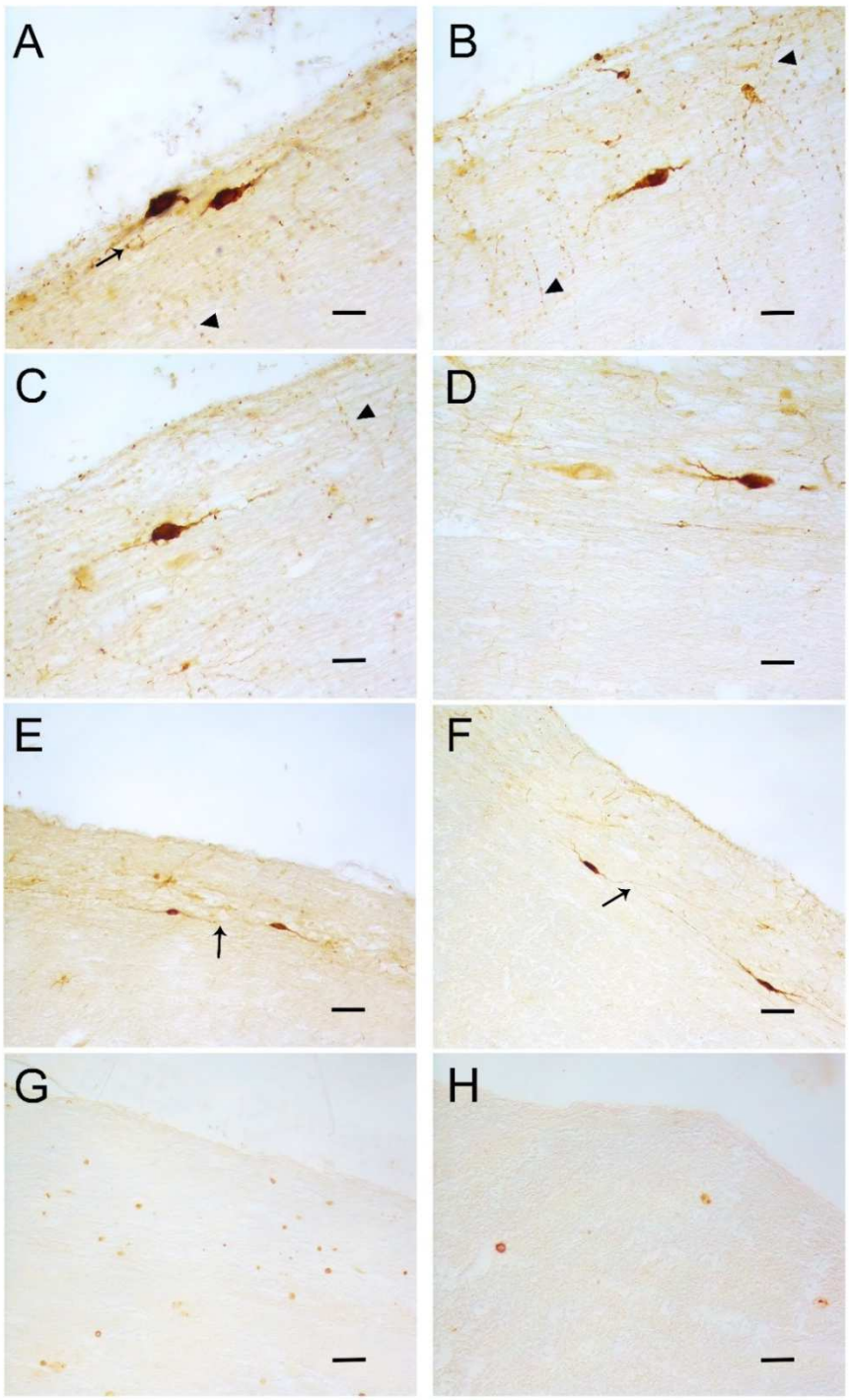

FIGURE 13

Photomicrographs of nNOS-immunopositive neuronal-like cells found in the anterior portion of the human IG, in sagittal sections. A-F: Photomicrographs showing different morphological types of nNOS-immunopositive cells: ovoidal (A, B, D), round (C), and fusiform (E, F). All these cells are bipolar and oriented horizontally. Neuronal NOS-positive fibres crossing the CC are indicated by arrow heads in A-C. Neuronal-like cells are close to each other and seem to establish a contact between them (A, E, F, black arrows). G, H: NeuN-immunopositive nuclei in IG. Calibration bars: A-C, D, H, 25µm; E-G, 50 µm.

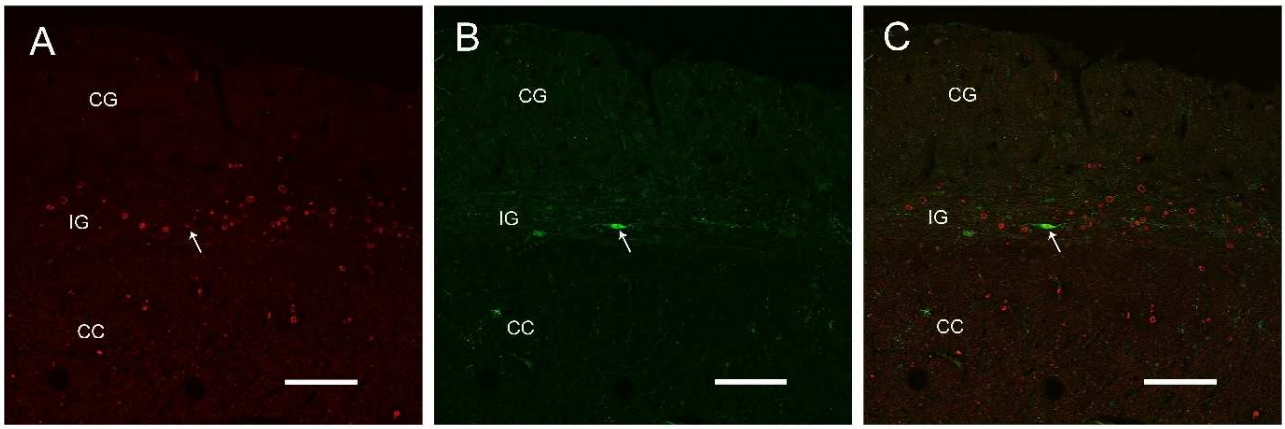

FIGURE 14

Confocal laser scanning photomicrographs. A NeuN-positive cell (A, white arrow) is also positive to nNOS (B, white arrow). C, merged image. Three layers, Cingulate Gyrus (CG), Indusium Griseum (IG) and Corpus Callosum (CC) can be distinguished also by the staining with Rhodamine phalloidin. Calibration bars: 100 µm.

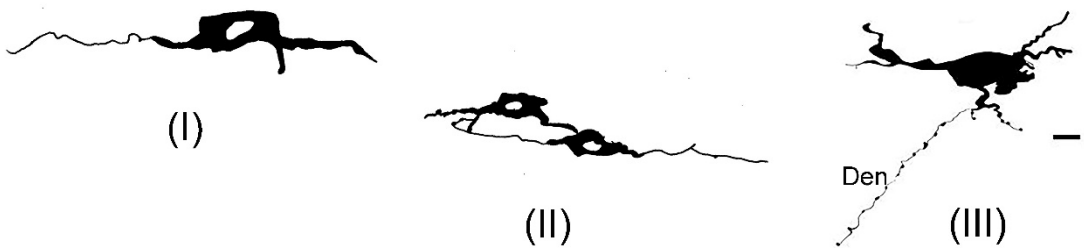

FIGURE 15

Camera lucida drawings of nNOS immunopositive neurons in the human IG. Three morphological types are shown: rectangular, I; ovoidal, II; round, III, with a long dendrite fiber (Den). Calibration bar I-III, 10 µm.

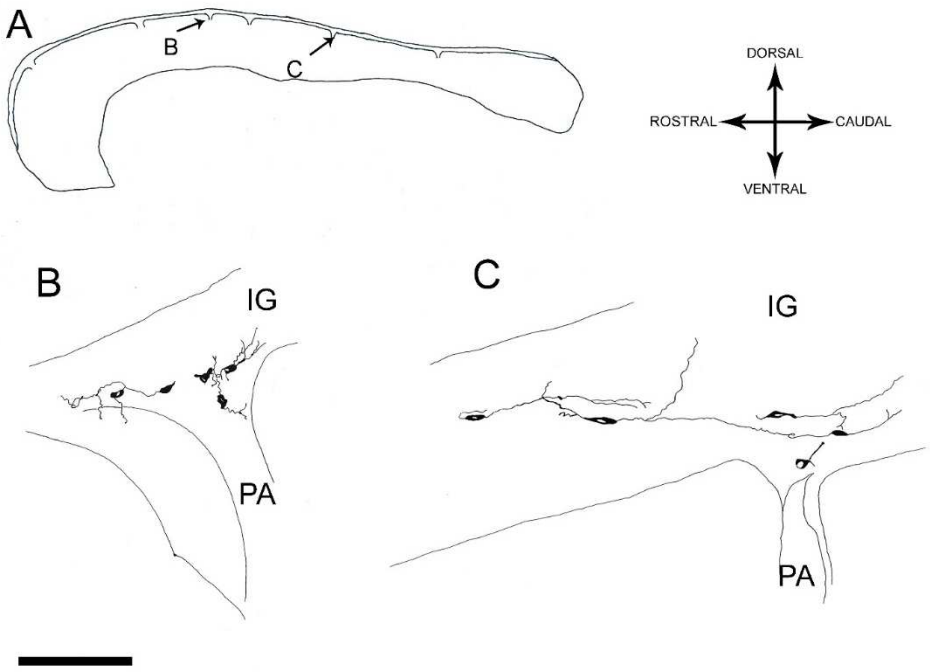

FIGURE 16

Outline figure of CC and overlying IG. The distribution of nNOS-positive neurons in IG is shown A; two regions are indicated (B, C; arrows) enlarged in B, and C, showing the distribution of nNOS-positive neurons close to pial arterioles (PA). Calibration bars A, 1 cm; B and C, 100 µm.

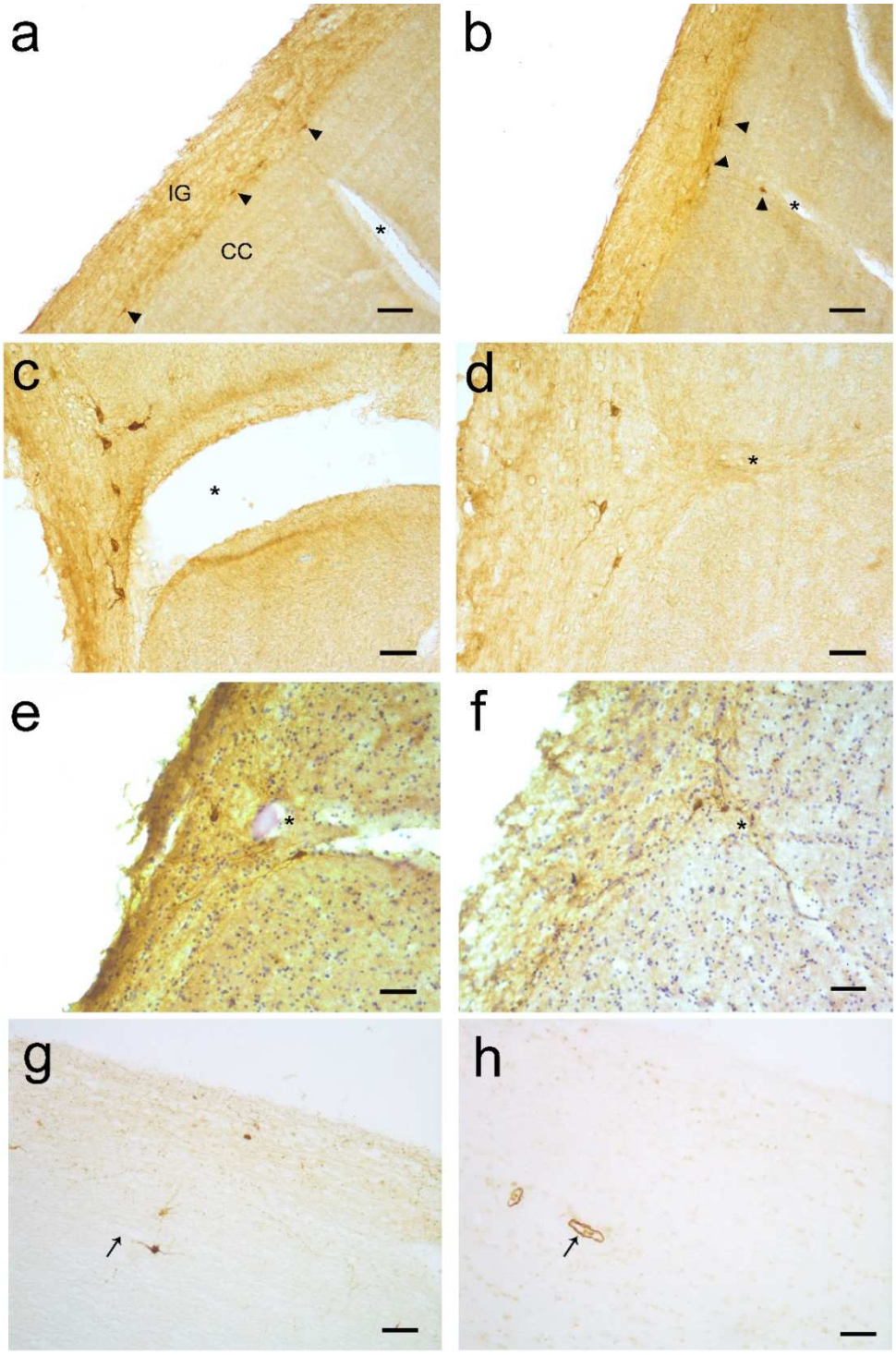

FIGURE 17

Photomicrographs show nNOS-positive neurons close to pial arterioles. A, B: low power magnification of nNOS-immunopositive neurons (arrow heads), nearby pial arterioles (asterisks). C-F: bipolar neurons around pial arterioles (asterisks) at higher magnification. Sections showed in E and F have been counterstained by hematoxylin to highlight the arterioles. Neurons in proximity of pial arterioles seem to be restricted in the lower portion of IG. G, H: a nNOS-immunopositive neuron and an αSMA-immunopositive arteriole shown in two serial sections: a close association of neuron with the vessel can be observed (arrow). Calibration bars: A and B, 100 µm; C-H, 50 µm

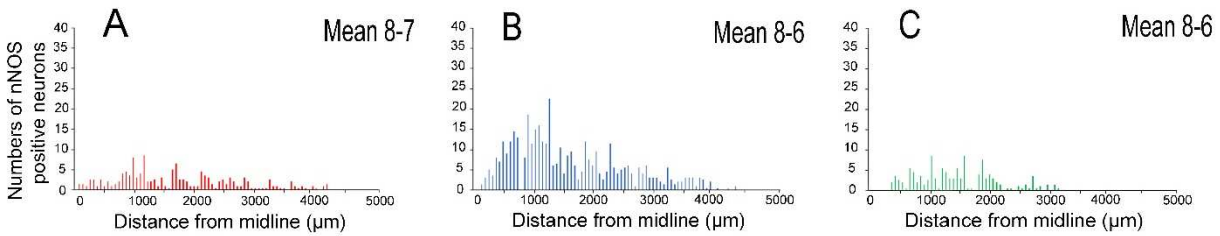

FIGURE 18

Histograms reporting the mean distribution of nNOS-immunopositive neurons along their medio-lateral dimension in the whole human IG (right hemisphere), as counted above callosal genu (A), callosal body (B) and callosal splenium (C) from 3 Cases (6, 7, and 8).

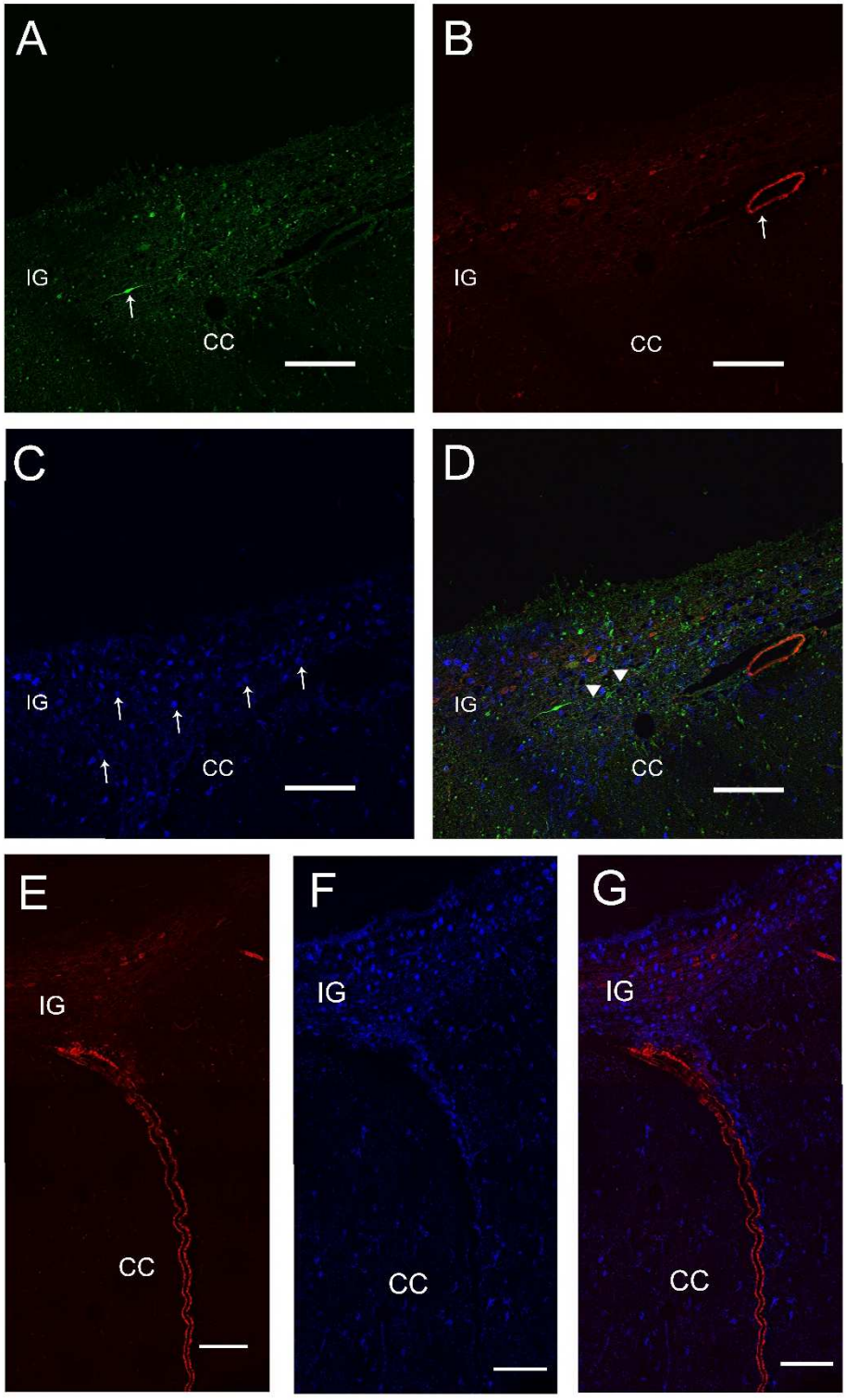

FIGURE 19

Confocal laser scanning photomicrographs. A-D and E-G represent two sagittal sections of human IG. A, nNOS-positive neuron (green; arrow); B, αSMA-positive arteriole (red; arrow); C, GFAP-positive astrocytes (blue; arrows); D, merged image showing also a fiber from the nNOS-positive neuron towards the αSMA-positive arteriole, marked by arrow heads; E, αSMA-positive arteriole (red); F, GFAP-positive astrocytes (blue); G, merged image. Calibration bars: 100 µm.

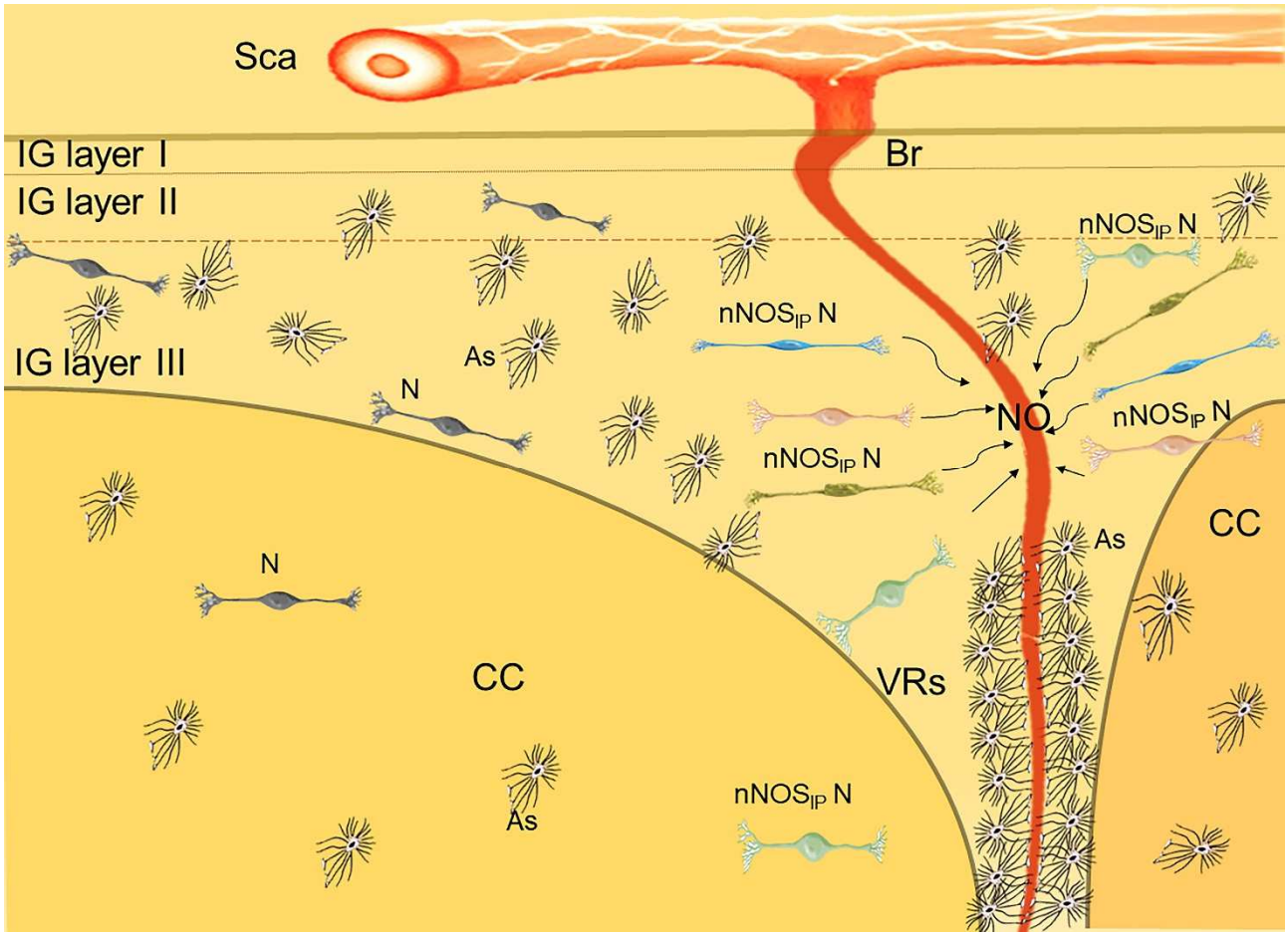

FIGURE 20

Schematic representation of the neurovascular unit composed by sopracallosal artery (Sca) that branches into smaller arterioles (Br). The arterioles cross the three layer of IG (layers I, II and III) and penetrate into the CC, separated from IG by the Virchow-Robin space (VRs). As the arterioles go deeper, this space disappears and the vascular basement membrane comes into direct contact with the astrocytic end-feets (intracallosal arterioles and capillaries). Neuronal NOS-immunopositive neurons (nNOS$_{IP}$ N) surround the arterioles and control the vasomotore tone by secreting nitric oxyde (NO). Four morphological types of nNOS$_{IP}$ N can be appreciated, labeled with different colors: fusiform (blue), rectangular (green), round (light green), ovoidal (pink). NeuN-immunopositive neurons (N) and many astrocytes (As) are also present, more numerous in IG than in CC.

10. TABLES

Table 1. Subjects' data and tissue processing for each brain.

Case n.	Sex	Age	Cause of Death	PMI (hours)	Western Blot	Immunohistochemistry		Immuno-fluorescence
						Paraffin sections	Frozen sections	
1	F	28	Hanging	24		x		x
2	F	38	Traumatic vertebral injury after fall	48		x		
3	M	51	Drowning	24		x		
4	M	61	Acute myocardial infarction	72		x		
5	M	79	Electromechanical dissociation	48		x		
6	F	41	Thoraco-abdominal injuries in road traffic accident	48		x	x	
7	F	43	Hemorrhagic shock in road traffic accident	48		x	x	
8	F	40	Traumatic brain injury in road traffic accident	96		x	x	x
9	M	54	Overdose	48		x		x
10	M	57	Plastic bag suffocation	48	x	x		
11	F	39	Inhalation of toxic products of combustion and carbon monoxide poisoning	72	x	x		
12	F	40	Electrocuted	24		x		
13	M	48	Shot	24		x		
14	M	30	Heart attack	48		x		
15	M	14	Hanging	72		x		
16	M	6	Traumatic asphyxia due to mouth compression	120		x		
17	M	81	Mesothelioma cachexia	168		x		
18	F	69	Hemorrhagic shock	168		x		
19	M	84	Ingestion of chemical substances (bleach)	24		x		
20	M	74	Lung mesothelioma	96		x		

Table 2. Primary antibodies used in the study.

Label	PrimaryAntibody	Supplier/ location	Polyclonal / Monoclonal	Immunogen	Dilution (µl)	Catalog #	RRID
nNOS	Rabbit anti-human neuronal Nitric Oxide Synthase	Cayman Chemical, Hambrug, Germany	Polyclonal	Synthetic peptide from the C-terminal region of human nNOS	1/700 for WB† 1/500 for IHC‡ and IF§	160870	AB_10080041
NeuN	Mouse anti-human Neuronal Nuclei	Merck, S.p.a., Milano, Italy	Monoclonal	Purified cell nuclei from mouse brain	1/100 for IHC and IF	MAB 377	AB_177621
α-SMA	Mouse anti-human alpha-Smooth Muscle Actin	Agilent Dako, Santa Clara, CA, USA	Monoclonal	SDS extracted protein fraction of human myocardium	1/100 for IHC and IF	M0635	AB_2242301
GFAP	Goat anti-human Glial Fibrillary Acidic Protein	Merck, S.p.a., Milano, Italy	Polyclonal	Peptide with sequence C-DGEVIKESK QEHKD from the C Terminus of the protein sequence according to NP_002046.1	1/100 for IF	SAB2500 462	AB_10603437
GFAP	Rabbit anti-human Glial Fibrillary Acidic Protein	Merck, S.p.a., Milano, Italy	Polyclonal	Purified bovine GFAP	1/1000 for IHC	AB5804	AB_2109645
GFAP	Mouse anti-human Glial Fibrillary Acidic Protein	Abcam, Cambridge, UK	Monoclonal	Full length native protein (purified) corresponding to Pig GFAP. A preparation of purified pig spinal cord GFAP.	1/500 for IF	ab4648	AB_449329

† Western Blot
‡ Immunohistochemistry
§ Immunofluorescence

Table 3. Secondary antibodies used in the study.

Label	Secondary antibody	Supplier/location	Dilution (µl)	Catalog #	RRID
Horserdish peroxidase	Donkey Anti-Rabbit	Amersham Italia srl, Milano, Italy	1/5000	NA934	AB_772206
Biotinylated	Goat anti-Rabbit	Vector Laboratories, Burlingame, CA	1/200	BA-1000	AB_2313606
Biotinylated	Goat anti-Mouse	Vector Laboratories, Burlingame, CA	1/200	BA-9200	AB_2336171
Alexa Fluor® 488	Goat Anti-Rabbit	Abcam, Cambridge, UK	1/200	ab150077	AB_2630356
Alexa Fluor® 555	Goat Anti-mouse	Abcam, Cambridge, UK	1/200	ab150114	AB_2687594
Alexa Fluor® 647	Donkey Anti-goat	Abcam, Cambridge, UK	1/200	ab150131	AB_2732857

Table 4. The absolute number of nNOS-positive neurons in the three callosal zones of each cases is shown, as wel the total number, the mean and the percentages.

Case	Genu	Body	Splenium	Total
6		137	108	245
7	64			64
8	125	438	173	736
Total	189	575	281	1045
Mean	95	288	141	524
%	18	55	27	100

Table 5. Autopsy data from selected cases.

Case n.	Sex	Age	Cause of Death	Agonal time (At)		PMI
				At < 10 min	10 min < At < 24 hours	
1	F	28	Hanging	x		24
2	F	38	Traumatic vertebral injury after fall	x		48
3	M	51	Drowning		x	24
4	M	61	Acute myocardial infarction	x		72
5	M	79	Electromechanical dissociation		x	48
6	F	41	Thoraco-abdominal injuries in road traffic accident		x	48
7	F	43	Hemorrhagic shock in road traffic accident		x	48
8	F	40	Traumatic brain injury in road traffic accident		x	96
9	M	54	Overdose		x	48
10	M	57	Plastic bag suffocation		x	48
11	F	39	Inhalation of toxic products of combustion and carbon monoxide poisoning		x	72

Table 6. Semi-quantitative evaluation of nNOS expression by immunohistochemistry.

Case n.	Number of nNOS positive cells	
	At< 10 min	**10 min < At< 24 hours**
1	-	
2	-	
3		++
4	-	
5		++
6		+
7		+
8		+
9		++
10		+
11		++

Table 7. Absolute number and percentage of nNOS-positive neurons in the different IG zones above the CC.

Case	Anterior IG	Middle IG	Posterior IG	Total
6		98	55	153
7	86			86
8	168	725	173	1066
Total	254	823	228	1305
Mean	127	412	114	653
%	19	63	18	100

11. SCIENTIFIC ARTICLES PRODUCED

- Lorenzi T, Sagrati A, Montanari E, Tagliabracci A, Barbaresi P, Fabri M, Morroni M. (2019). Letter: The Indusium Griseum: Anatomic Study with Potential Application to Callosotomy. Neurosurgery, 1;85(3):E621-E622. doi: 10.1093/neuros/nyz236.

- Lorenzi, T., Sagrati, A., Montanari, E., Senzacqua, M., Morroni, M., Fabri, M. (2021). Hypoxia-induced expression of neuronal nitric oxide synthase in astrocytes of human corpus callosum. Brain Struct Funct, 226:1353-1361, doi: 10.1007/s00429-021-02244-5.

Submitted:

- Lorenzi, T., Sagrati, A., Montanari, E., Senzacqua, M., Morroni, M., Fabri, M. (2021) Characterization and quantification of neuronal nitric oxide synthase neurons in human indusium griseum.

In preparation:

- Sagrati, A., Lorenzi, T., Montanari, E., Senzacqua, M., Morroni, M., Fabri, M. Characterization and quantification of neuronal nitric oxide synthase neurons in human corpus callosum.

12. RINGRAZIAMENTI

Questa tesi di dottorato non avrebbe mai visto la luce senza la disponibilità e la pazienza del primo tutor, la Professoressa Mara Fabri, che ringrazio sinceramente e cordialmente per avermi dato l'opportunità di entrare a contatto con il mondo della ricerca. Un grazie particolare va al secondo tutor, la Dottoressa Teresa Lorenzi, di enorme aiuto scientifico che fin dalle primissime fasi di elaborazione mi ha incoraggiato in tutti i modi possibili a continuare a lavorare, vedendo nelle mie riflessioni potenzialità che io stesso, all'inizio del lavoro, faticavo a scorgere e per avermi guidato nel mio percorso di ricerca con preziosi consigli.

Ringrazio inoltre la Dottoressa Eva Montanari per l'aiuto nella raccolta campioni.

Ringrazio altresì il Professore Paolo Barbaresi, che ha sempre considerato con simpatia e partecipazione il mio operato scientifico e non mi ha mai fatto mancare preziosissimi consigli atti a portare avanti il lavoro.

Infine ringrazio il Professore Slobodan Petar Malobabic per i commenti della tesi.